HYDROGEN METAL INTERACTION IN Fe-Al INTERMETALLICS

by

PRAVIN DHAWAD

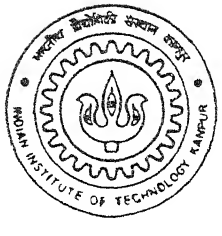

DEPARTMENT OF MATERIALS AND METALLURGICAL ENGINEERING

INDIAN INSTITUTE OF TECHNOLOGY, KANPUR

JULY, 1998

HYDROGEN METAL INTERACTION IN Fe-Al INTERMETALLICS

A Thesis Submitted

in Partial Fulfillment of the Requirements

for the Degree of

Master of Technology

by

PRAVIN DHAWAD

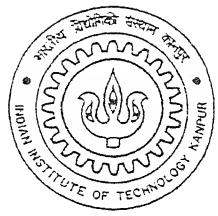

DEPARTMENT OF MATERIALS AND

METALLURGICAL ENGINEERING

INDIAN INSTITUTE OF TECHNOLOGY

KANPUR 208 016

JULY 1998

Entered In System.

ACKNOWLEDGEMENT

I wish to take this oppurtunity to express my heartfelt reverence and deep sense of grattitude to my supervisors Professor K. N. Rai and Dr. V. N. Kulkarni for their expert guidence, valuable suggestions, continuous encouragement and granting me personal freedom throughout the entire programme which brought forth the culmination of the study.

I wish to express my sincere appreciation of monumental help and suggestions obtained from Dr. M. N. Mungole during my experiments.

I am grateful to Mr. P. K. Paul, Mr. Agnihotri, Mr. Jain and Mr. Umashankar for their help at crucial moments.

I deeply cherish the affection showered on me by my dear friends Mangesh, Bhupesh, Shivraj, Sameer, Pushkar and Parag. Cooperation and help received from Prasad, Arvind and Amit are thankfully acknowledged.

I owe my fruitful stay at I.I.T. Kanpur to all my classmates, wingmates and Mathoo friends.

I had also the privilege to be associated with many other friends and well wishers whose names have not been mentioned here.

Continued encouragements received from Professor G. S. Upadhyay and Professor Brahma Deo are also sincerely acknowledge.

I am grateful to Dr Mungole and his family members who with their affection and love made my stay a memorable one.

Finally I am greatly indebted to my beloved family members, relatives and friends whose continued encouragement, support and the patience they have shown during the entire programme enabled me to complete the study.

Pravin Dhawad

DEDICATED

TO

MY

BELOVED PARENTS

CONTENTS

CERTIFICATE

It is certified that the work contained in the thesis entitled "**Hydrogen metal interaction in Fe-Al intermetallics**", by **Pravin Dhawad** has been carried out under our supervision and has not been submitted elsewhere for a degree.

Dr. K.N.Rai,
Professor,
Material Science Programme
and Department of Materials
and Metallurgical Engineering,
Indian Institute of Technology,
Kanpur - 208016.

Dr.V.N.Kulkarni,
Assistant Professor,
Department of Physics,
Indian Institute of Technology,
Kanpur - 208016.

July 1998

SYNOPSIS

The present thesis is an attempt to give insights to the hydrogen intermetallic interaction. Various methods of hydrogen incorporation and its detection and depth profiling by Elastic Recoil Detection Analysis (ERDA) using 1.25 MeV $4He^{-}$ ion beam undertaken in the present work. It was noticed that the diffusion of ionic hydrogen is easier into this material in comparison to the atomic hydrogen. Molecular hydrogen does not diffuses into this material easily even at a temperature of $800^{0}C$ for hours. This study is the first attempt for the direct detection of hydrogen and deuterium in Fe-25 at % Al. Till now the most of the work on hydrogen diffusion was concentrated on Fe-40 at % Al.

The ERDA technique detected some amount of hydrogen in all the samples whether charged with hydrogen or virgin. This results probably provides direct support of the proposed mechanism that moisture induced hydrogen is the cause of severe embrittlement in iron aluminide. Nevertheless, direct measurement of trapped hydrogen in the bulk of the intermetallic alloy have not been reported in the literature earlier.

Convincing evidence is provided here for the hydrogen trapping in iron aluminide when charged and desorbs when heated in vacuum. This observation supports the hypothesis of hydrogen embrittlement reversibility due to thermal activation.

Magnetic study of iron aluminide revealed that addition of aluminium to iron reduces its magnetic saturation by simple dilution rule as observed by other workers. However, the magnetization curve, departs from linearity and the magnetic saturation

of electronic interaction between Al and Fe. Addition of Chromium was found to increase saturation magnetization due to addition of more vacant 3d band.

Magnetic saturation of iron aluminide was not affected with hydrogen the only exception being the iron aluminide containing chromium. In this sample the magnetic saturation was found to decrease after high temperature hydrogen charging. It was found that the addition of chromium to iron aluminide in the range 20 to 28 at % Al increases the DO3-B2 ordering transformation temperature. This finding can be used to detect DO3 to B2 transition temperature by magnetic measurements in addition to other methods.

LIST OF FIGURES

LIST OF TABLES

CHAPTER 1

INTRODUCTION

1.1 INTERMETALLICS

Ordered intermetallics constitute an unique class of metallic materials that form long-range-ordered crystal structures below a critical temperature which is generally referred to as the critical ordering temperature (Tc) [1]. The first studies on the iron-aluminium system was conducted in the 1930s [2]. These intermetallics usually exist in relatively narrow compositional ranges around simple stoichiometric ratios. The search for new high-temperature structural materials has stimulated much interest in ordered intermetallics. Intermetallic aluminides possess many attributes that make them attractive for high temperature structural applications [1]. In oxidizing environments they contain enough aluminium to form, thin films of aluminium oxides that are often compact and protective. They have low densities, relatively high melting points and good high strength properties.

The aluminides that have attracted attention for potential application as high temperature materials are titanium, nickel and iron aluminides. The present trend of investigation on these aluminides in the recent past is on an upswing due to their possible application at high temperatures. Because of this importance I have undertaken the task of further studies on the aluminides of Fe-Al system. Following sections of this manuscript therefore describe in short, the work on iron aluminide of our interest and the aim of further investigation on this materials.

1.2 IRON ALUMINIDES

Ordered iron aluminide intermetallics of composition Fe_3Al and FeAl possess attractive properties for application at elevated temperatures and severe environments over structural materials like stainless steels and nickel-base super alloys. Specific advantages include: (1) excellent sulphidation resistance, (2) oxidation resistance, (3) lower density, (4) good wear resistance, (5) cavitation erosion resistance and (6) potentially lower cost [1]. However, their poor room temperature ductility limits their use as engineering materials as they are difficult to process into useful shapes like plates, wires and tubes. However, in recent years, efforts have been intensified to identify both the extrinsic and intrinsic factors governing room temperature brittle fracture.

It has now been firmly established that the poor room temperature ductility is caused mainly by an extrinsic effect-environmental embrittlement due to hydrogen [3]. Hydrogen is produced due to the reaction of the fresh surface of iron aluminide with moisture and therefore, the poor ductility has also been attributed to moisture-induced embrittlement. Direct evidence for the production of hydrogen on reaction with water has been recently produced [4].

Several methods have been proposed to minimize hydrogen embrittlement (HE) in iron aluminides as it is well known that environmental effect is responsible for the poor room temperature ductility and fracture mode in Fe_3Al [5]. Most of the methods that have been suggested to curb HE aim to restrict entry of hydrogen into the lattice. A good method for improving the ductility of iron aluminides is by the addition of chromium [6-8]. Even small chromium additions are effective in minimizing hydrogen embrittlement and in providing increased ductility [6]. Oxide [7] and metallic [9]

coatings have been beneficial in increasing the ductility of iron aluminides. Thermomechanical treatments also play a very crucial role in determining the mechanical properties of iron aluminides [10]. Finally improving the ductility of iron aluminides by alloying with passivity-inducing elements [8, 11] has also been suggested as one of the methods.

It has been proposed by Balasubramaniam that alloying Fe_3Al with passivity-inducing elements would reduce hydrogen liberation rates on the surfaces of iron aluminides and the passive layer further hinder the diffusion of hydrogen into the intermetallic, thereby minimizing HE [8]. The role of surface passive films on the HE of iron aluminides has been reviewed recently [12]. Nine passivity-inducing elements were alloyed to Fe_3Al to produce intermetallics of composition Fe-24Al-5M where M = Ti, Zr, V, Nb, Ta, Cr, Mo, W and Si [13]. Only the base Fe_3Al, Cr- and Ti-alloyed intermetallics could be processed to 80% deformation at 1000^0C. The role of thermomechanical treatments on the room temperature tensile behavior of Fe_3Al has been earlier studied in detail [10]. It was seen that stoichiometric Fe_3Al obeys the Hall-Petch relationship [14]. The Cr- and Ti-alloyed intermetallics also exhibited ductility at room temperature [13]. Barring the base Fe_3Al and Fe_3Al-5V intermetallics, all the others exhibited active-passive behaviour in 0.05 mol/l H_2SO_4 solution. Alloying with Cr and Ti should be beneficial in improving the ductilities. Incidentally, the alloy development to develop ductile iron aluminides has also been reviewed by Balasubramaniam [11].

1.3 AIM OF THE STUDY :

Hydrogen is notorious for embrittlement in iron aluminide. It has been well established that the poor room temperature ductility of iron aluminide is mainly due to

hydrogen embrittlement. Iron aluminide is intrinsically ductile but the extrinsic factors like presence of hydrogen makes it brittle. As noted above several methods have been proposed to minimize embrittlement.

It has been hypothesized that the hydrogen is generated by the reaction of fresh surface of iron aluminide with water and iron aluminide can be charged cathodically. It has been also proposed that the hydrogen embrittlement is completely reversible. This can be achieved by thermal desorption of H_2 in vacuum.

One of the aims of the present investigation was to check the validity of these hypothesis upto certain extent.

Primary aim was to directly quantitize the amount of hydrogen and deuterium diffused into the iron aluminide unlike other workers who have tried to correlate it with changes in microhardness measurements and ductility.

The present thesis work deals with the detection of hydrogen and its depth profiling by elastic recoil detection analysis (ERDA) using 1.25 MeV $4He^{+}$ ions in iron aluminide after different hydrogen incorporation methods viz plasma ion irradiation, cathodic hydrogen charging, hydrogen gas charging at high temperature followed by desorption studies on iron aluminide.

As the state of alloying is associated with changes in magnetic properties of this material, work on magnetization studies have been carried out. It involves average atomic magnetic measurements and the curie temperature evaluation.

1.4 PLAN OF WORK :

The hydrogen charging of iron aluminide was carried out by adopting all the three methods viz (i) cathodic, (ii) plasma and (iii) gas charging. Both isotopes, the hydrogen and deuterium were used for the present work. The quantitative evaluation

of these species in intermetallics were carried out using method of Elastic Recoil Detection Analysis (ERDA).

Iron aluminide is ferromagnetic. Since hydrogen diffusion in iron aluminide alters the magnetic property of iron aluminide especially the magnetic saturation, magnetic study on iron aluminide was carried out in magnetics lab to quantitize the amount of hydrogen diffused into the iron aluminide. In this connection iron aluminides of different aluminium concentration were borrowed from the students working on the iron aluminide and their magnetic saturation study was also undertaken.

ERDA using Van De Graff accelerator at central nuclear lab is the only world wide acclaimed direct and non destructive method of determining hydrogen and its isotopes diffusivity in the material. Plasma ion implantation along with the thermal annealing of hydrogen charged sample in vacuum was also carried out in the nuclear lab of I.I.T. Kanpur. Heavy water D2O from BARC was available in the material design and development lab. Hence iron aluminide was cathodically charged with D2O in order to verify the validity of our studies.

CHAPTER 2

LITERATURE REVIEW

The intermetallics of Iron-Aluminium are important candidates for structural materials at high temperature because of their inherent oxidation resistance, high strength to weight ratio but it is susceptible to hydrogen embrittlement. This section deals with the role of hydrogen in affecting the room temperature ductility, with special reference to hydrogen embrittlement mechanism, hydrogen trap interaction and hydrogen diffusivity. The methods that have been utilized to provide enhance ductility to iron aluminide are briefly discussed here.

2.1 PHASE DIAGRAM AND STRUCTURES

Ordered iron aluminides exist in relatively narrow compositional ranges around simple stoichiometric ratios (Figure 1). Iron Aluminides based on Fe_3Al and FeAl can exist in two crystal allotropic modifications. These structures (DO_3 and B2) are both ordered BCC structures and these are presented in Figure 2. Fe_3Al can exist both as B2 and DO_3 ordered structure depending upon the temperature (Figure 1) while FeAl can exist only in the B2 ordered form [1]. Table 1 presents some typical room temperature properties and critical ordering temperatures for different allotropic modifications of iron aluminides [1].

2.2 ROOM TEMPERATURE MECHANICAL BEHAVIOUR

Iron aluminides have been known to be brittle at room temperature since 1930 [2]. However, the major cause of their low ductility and brittle fracture was not known. Recently, Liu *et al* have proposed an environmental effect as the major cause for room temperature embrittlement in iron aluminides [3]. They proposed that the

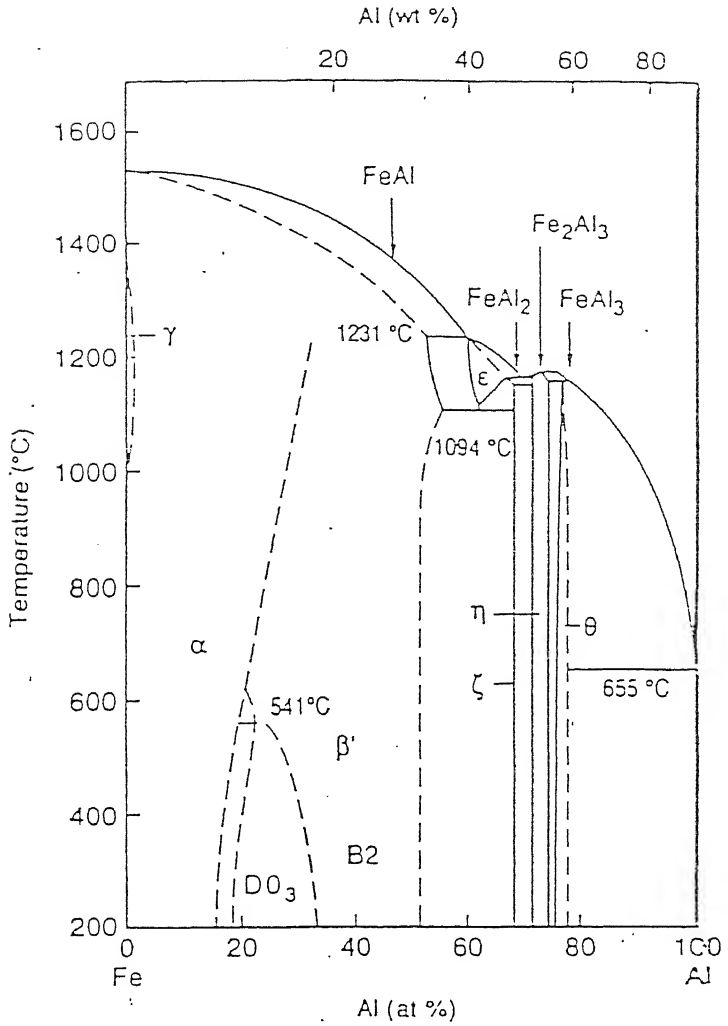

Figure 1. The Fe-Al phase diagram.

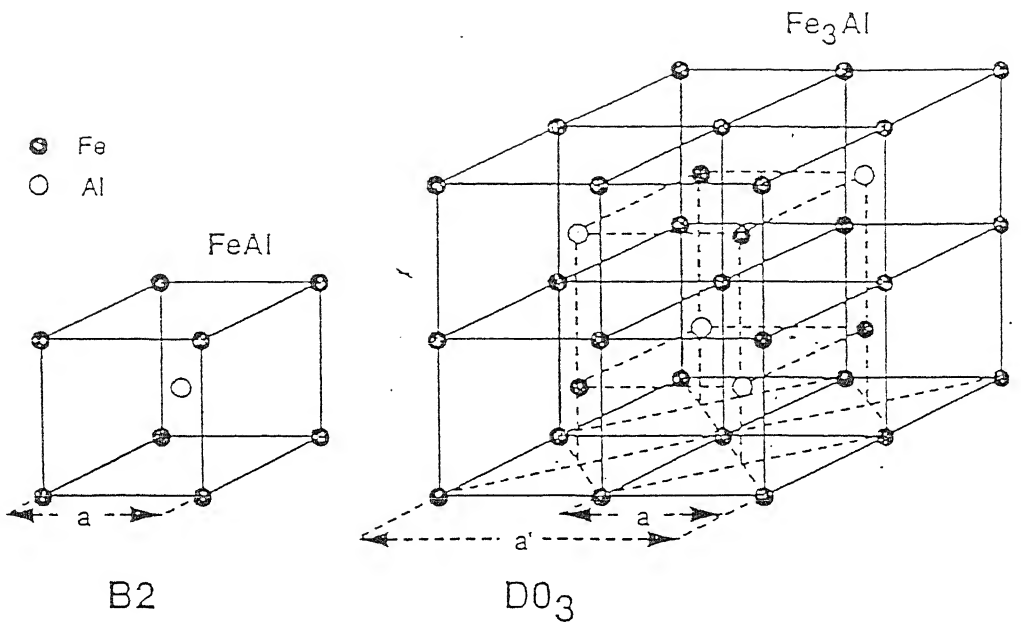

Figure 2. The DO_3 and B2 ordered crystal structure of iron aluminide.

Table 1. Typical room temperature properties of iron aluminides [1].

Alloy	Crystal Structure	Temp. (°C)		Density (gm/cc)	Room Temp. Y.Strength (MPa)	Room Temp. Elongation (%)
		order-ing	M.P.			
Fe_3Al	DO_3	540	1540	6.72	300	3.7
Fe_3Al	B2	760	1540	6.72	380	4.1
FeAl	B2	1250	1250	5.56	360	2.2

embrittlement involves the reaction of water vapor with aluminum atoms and releases atomic hydrogen which enters the lattice and causes embrittlement. Direct evidence has also been recently provided for the production of hydrogen by reaction of iron aluminide with water vapor by Zhu *et al* [4] by a laser mass spectroscopic technique.

That hydrogen is the main damaging agent causing poor ductility was confirmed from tensile tests conducted in different environments. These results are summarized in Table 2 [5]. The effect of various test environments on the room temperature stress-strain behaviour of iron aluminides is shown schematically in Figure 3 [12]. As evident from Figure 3, ductility is higher in Ar + 4% H_2 environment rather than humid air. This is because molecular hydrogen does not cause much embrittlement in Fe_3Al, because of its lower activity as compared with atomic hydrogen produced from water vapor environment show least ductility and vacuum/oxygen environments provide high ductility. Liu *et al* have shown that higher ductilities are observed in a dry oxygen environment rather than in vacuum because oxygen reacts with aluminum to form Al_2O_3 directly [5]

$$2Al + 3/2\ O_2 = Al_2O_3 \qquad (1)$$

and thereby suppressing the aluminum-moisture reaction which provides nascent hydrogen.

$$2Al + 3H_2O = Al_2O_3 + 6H \qquad (2)$$

Generation of atomic hydrogen is suppressed and thus higher ductility is observed in dry oxygen environment.

One of the most crucial factors to be understood for improving the room temperature mechanical properties of iron aluminides, especially the ductility, is the entry of hydrogen into the material. A factor that is of secondary importance is the

Table 2. Room temperature tensile properties of iron aluminides in different test environments [5].

Environment	Yield Strength (MPa)	UTS (MPa)	Ductility (%)
	Heat Treated for 2 hr at 700°C (B2 Structure)		
Vacuum	387	851	12.8
Oxygen	392	867	12.0
Ar + 4% H_2	385	371	8.4
Air	387	559	4.2
H_2O vapour	387	475	2.1
	Heat Treated for 120 hr at 500°C (DO_3 Structure)		
Vacuum	316	813	12.4
Oxygen	298	888	11.7
Air	279	514	3.7
H_2O vapour	322	439	2.1

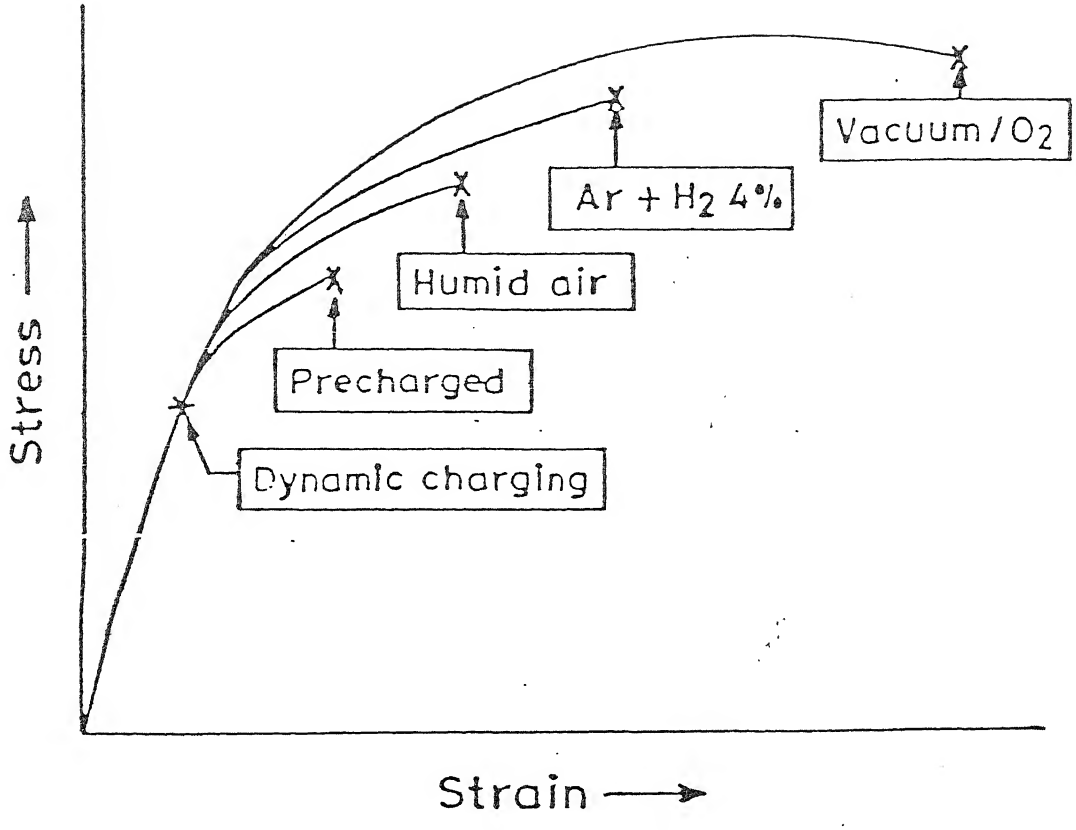

Figure 3. Schematic tensile stress-strain behaviour of iron aluminides in various environments at ambient temperature.

diffusivity of hydrogen through the aluminide because hydrogen has to diffuse and concentrate in certain specific regions of the aluminide in order to cause hydrogen embrittlement. The role of microstructure is also a factor that has to be reckoned while considering hydrogen diffusivity. These aspects would be reviewed in the following sub-sections.

2.3 DUCTILITY IMPROVEMENT METHODS

Several methods that have been utilized to improve the ductility of iron aluminides would be briefly discussed in this section. These methods include the following:

Alloying

Alloying addition has been one of the schemes used to improve the ductility of iron aluminides. Alloying controls surface condition, reduction in hydrogen solubility and diffusion, refinement of grain structure, enhancement of grain boundary cohesion, grain shape and recrystallization condition [1].

Of the several methods which have been adopted to minimize HE of iron aluminides, chromium additions have been very useful in increasing ductility by an order of magnitude [6-8]. McKamey and Liu have earlier suggested that the beneficial effect of Cr comes from surface oxide modification, rather than modification of bulk properties [7]. They suggested a change in oxide chemistry and properties or a change in the kinetics of oxide formation, thereby reducing the water-vapor reaction. The mechanism for the increase in ductility by Cr additions has been elucidated by the mixed potential theory by Balasubramaniam [8] wherein it was proposed that alloying with Cr induces passivity results in reduction in the rate of the hydrogen that enters the lattice to cause embrittlement. This mechanism suggests that the entry of hydrogen into

the lattice can be checked and HE minimized by alloying passivity-inducing elements (like Ti, Zr, V, Nb, Ta, Cr, Mo, W, Si and Ni) to iron aluminides [8].

Boron addition (in ppm range) has been found to be very effective in increasing the grain boundary cohesiveness in ordered B2 FeAl intermetallics [19]. It has been suggested that boron segregates to the grain boundaries and reduces the intrinsic brittleness of B2 FeAl, thereby minimizing HE [20].

Zirconium has been alloyed to Fe_3Al to strengthen grain boundaries and to prevent recrystallization [15]. McKamey and Pierce have already confirmed that partially recrystallized microstructure reduces hydrogen embrittlement [15]. Therefore, zirconium additions can help in minimizing hydrogen embrittlement.

Liu *et al* have studied the effect of Ti addition to Fe_3Al on the mechanical behavior of at high temperatures [21]. They have demonstrated super plastic behavior in the Fe_3Al-2Ti alloy at high temperature. This has been ascribed to the process of dynamic recovery and recrystallization occurring in Fe_3Al-2Ti intermetallic at high temperatures.

Yangshan *et al* [22] have shown that cerium additions to a very small extent increases the ductility of base Fe-28Al and Cr-alloyed iron aluminides significantly. They proposed that Ce additions accelerated the formation of aluminum and chromium oxides which passivated the specimen surface thus preventing hydrogen from diffusing into the specimen. Interestingly, the addition of Ce had also changed the composition of the surface passive film. With the addition of Ce, the surface layer contained a larger amount of Al_2O_3 and Cr_2O_3 and a lower amount of Fe_2O_3 than the Fe-28Al-2Cr alloy without Ce addition. They have also shown that Ce additions caused partially ductile failure instead of brittle failure in the iron aluminides without Ce additions. Addition of Ce also produced a fine grain structure after complete recrystallization in contrast to

the large grain size observed without Ce additions. Therefore, the strength properties were not significantly reduced upon complete recrystallization in the Ce-alloyed iron aluminides. They also observed precipitates rich in Fe, Al and Ce to form in the grain boundary regions of the Ce-alloyed intermetallics. It is reasonable to assume that the Ce-containing phase acts as irreversible traps for hydrogen and therefore, lowers the amount of hydrogen present in the material, thereby delaying embrittlement [11]. Therefore, the presence of strong hydrogen trapping compounds, homogeneously distributed through out the iron aluminide matrix, could also be beneficial in delaying embrittlement.

Recently, mischmetal (Mm) has also been alloyed in a small amount to Cr- and Ti-alloyed iron aluminides as one of the important elements in Mm is Ce [18, 23]. However, there was no enhancement in the ductility due to Mm additions and this has been attributed to the segregation the elements in Mm to the grain boundaries (which weaken the boundaries) and also to the precipitation of ternary brittle phases due to Mm addition.

Surface Modification

The surface nature can be manipulated by several methods such as (i) electropolishing, (ii) oxide coating, (iii) metallic coating and (iv) alloying. The first two aspects were studied in detail by McKamey and Liu [7] who found that ductility increases upon oxide coating. The samples which were electropolished and then annealed in vacuum to minimize oxide reformation show ductility comparable to the binary Fe-28Al intermetallic in both the B2 and DO_3 ordered conditions. There is a significant increase in ductility for Cr containing samples as compared to the base Fe-28Al intermetallic in the as rolled condition. Chromium containing specimen which were heat treated for 96 hours at 500^0C in air (to give the DO_3 crystal structure) show

comparable ductilities, whether they were oxide coated or present in the as rolled condition. Also, the ductility of the oxide coated (Cr containing) intermetallic is higher than the electropolished specimen. These results strongly suggest that surface passive films on iron aluminides restrict hydrogen embrittlement.

It has also been shown that metallic coatings of Cu and Ni on iron aluminide of composition Fe-28Al-5Cr-0.5Mo-O.5Nb-O.05B-O.05Zr are effective in minimizing the environmental embrittlement [9]. The coatings were applied by electro-brush plating. Plating with Cu was shown to be more effective in inhibiting embrittlement. The fracture morphology changed from transgranular cleavage for non-coated specimens to a mixed one of dimple fracture and transgranular cleavage for the coated specimens. An inner layer was found between the copper coating and the matrix which was formed by reaction of the copper with the iron aluminide matrix. The role of surface films in minimizing HE has been reviewed by Agarwal and Balasubramaniam [12].

Partial Recrystallization

The control of grain size is important in determining the mechanical properties of iron aluminides [14]. Moreover, the ductility is influenced by the type of recrystallization microstructure. The effect of annealing on room temperature technical behaviour of iron aluminides is discussed in greater detail in the following section.

2.4 ANNEALING EFFECTS ON MECHANICAL BEHAVIOUR OF IRON ALUMINIDE

In addition to the environmental effects, the strength and ductility of iron aluminide are strongly affected by the processing schedule, the cooling rate from the high temperature and the heat treatment provided at high temperatures. Improvements in ductility have been obtained by low temperature annealing heat treatments [15, 24-30]. In such cases, the ductility obtained after annealing heat treatments is significantly greater than that immediately after mechanical forming and is about double that obtained following complete recrystallization at higher temperatures [26]. Since the strength remains high after the low temperature annealing heat treatments, the end result is a strong material of greatly improved ductility.

It has been observed that ingot metallurgy route followed by thermomechanical treatments significantly increases the tensile properties [24]. It is also observed [25] that the Fe-24.6Al alloy, rolled and heat treated at 700^0C for 1h, exhibited a good combination of tensile properties like ductility, yield strength (YS) and ultimate tensile strengths (UTS). It has been hypothesized that this could be due to subgrain structure formation and/or due to the partial recrystallization, the reason being not clear [25]. Moreover, a partially recrystallized structure is beneficial compared to a fully recrystallised as regards ductility [15]. This is evident from the Table 3 [15] that recrystallisation plays a dominant role in improving the tensile properties of iron aluminide. In view of the above, the recrystallization structure of iron aluminide influences room temperature ductility.

The recrystallisation process vary greatly in the iron aluminide system with several variables such as thermomechanical treatments, alloying, crystal structure,

Table 3. Effect of annealing temperature on room temperature properties of iron aluminides [15].

Heat treatment[b] (h/°C)	Fraction recrystallized (%) (grain size, μm)	Yield stress (MPa)	Fracture stress (MPa)	Elongation (%)
1/550	0	550	760	5.4
1/650	0	543	807	8.1
1/750	10	479	736	8.0
1/850	20	453	670	6.4
1/1000	100 (41)	280	413	3.0
1/1100	100 (68)	279	450	4.0
0.5/750	<5	481	736	8.2
1/750	10	466	710	7.8
4/750	25	438	665	7.8
24/750	50 (20-30)	369	577	5.2
48/750	80 (20-60)	328	492	4.4
0.17/1000	100 (34)	288	439	3.6
0.5/1000	100 (36)	287	425	3.0
1/1000	100 (43)	274	436	3.2
4/1000	100 (45)	277	422	3.0

[a]Alloy composition, Fe-28Al-5Cr-0.1Zr-0.05B (at.%).
[b]All alloys were heat treated 1 h at 700°C before punching test specimens. After the recrystallization heat treatment, all specimens were annealed for 3 d at 500°C to establish DO_3 order.

microstructure and type and amount of order [31, 32]. It is very difficult to predict precisely the recrystallisation temperature and kinetics in Fe_3Al system [31-33]. The effect of recrystallization is further elucidated in Figures 4 [15], 5 [21], 6 [25], 7 [29], 8 [26] abd 9, 10 [28].

Figure 4 [15] shows that ductility improves after annealing at 750^0C for one hour. This treatment produces a stress relieved but partially recrystallised microstructure. Table 3 and Figure 4 also reflect that increasing the degree of recrystallisation results in loss of ductility and tensile strength. A completely recrystallised microstructure produces the least desirable mechanical properties. It is obvious from Figure 4 that the best room temperature tensile strength and ductility was obtained in specimen which had been heat treated to relieve stress produced by fabrication and had a minimum number of recrystallised grains [15]. The super plastic behaviour of Fe_3Al alloy containing titanium as shown in Figure 5 [21] is suggested to be due to dynamic recrystallisation taking place at high temperatures in presence of titanium. The temperature of annealing is also important in determining the ductility at room temperature (Figure 6 [25]). Moreover, as the recrystallization annealing affects the mechanical properties, it is expected that the processing temperature would also play a role in determining the room temperature ductilities. Figure 7 [29] indicates that the best combination of tensile properties are obtained in the processing temperature range of 700^0C to 800^0C, which is thought to be due to the partial recrystallisation taking place in addition to recovery to form the subgrain structure, in this temperature range. Moreover, the grain size is also a function of the annealing temperature (Figure 8 [26]) and this would affect the mechanical properties as iron aluminides obey the Hall-Petch relationship [14]. Optimum yield stress and ductilities were obtained after

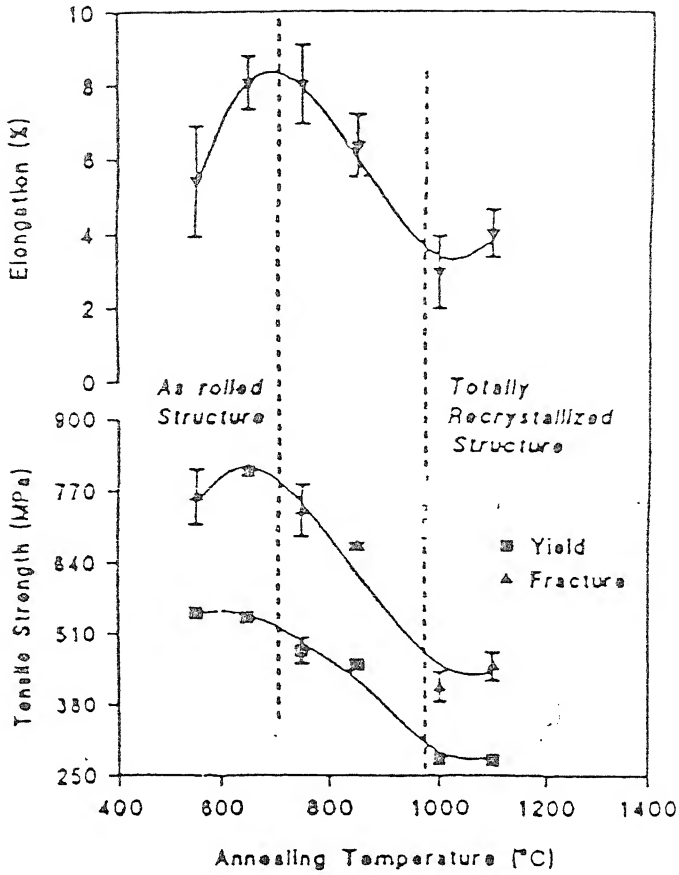

Figure 4. Effect of annealing temperature on room temperature properties of iron aluminides [15].

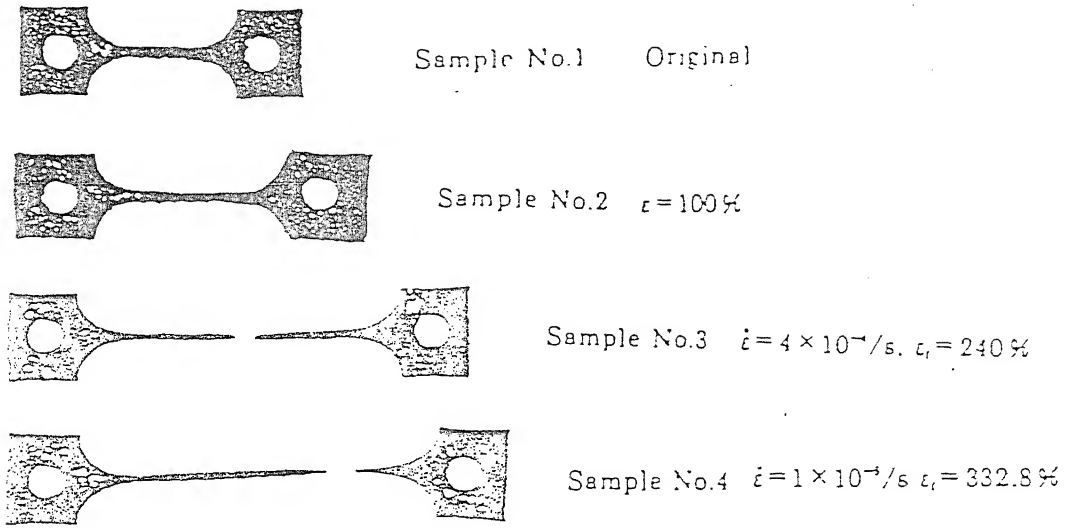

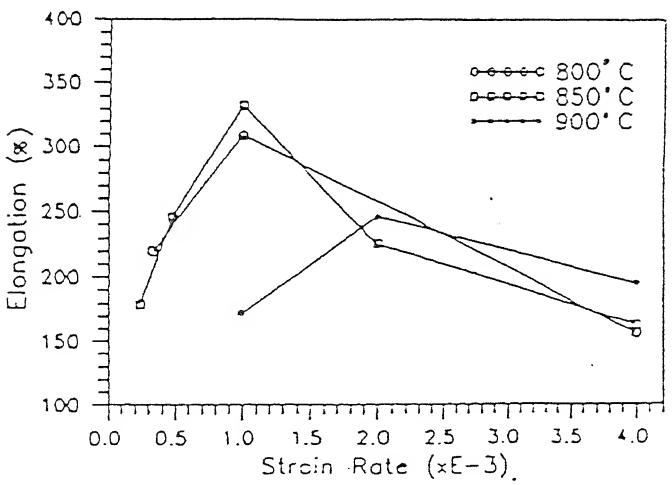

Figure 5. Superplastic behaviour in Fe-28Al-2Ti alloys [21].

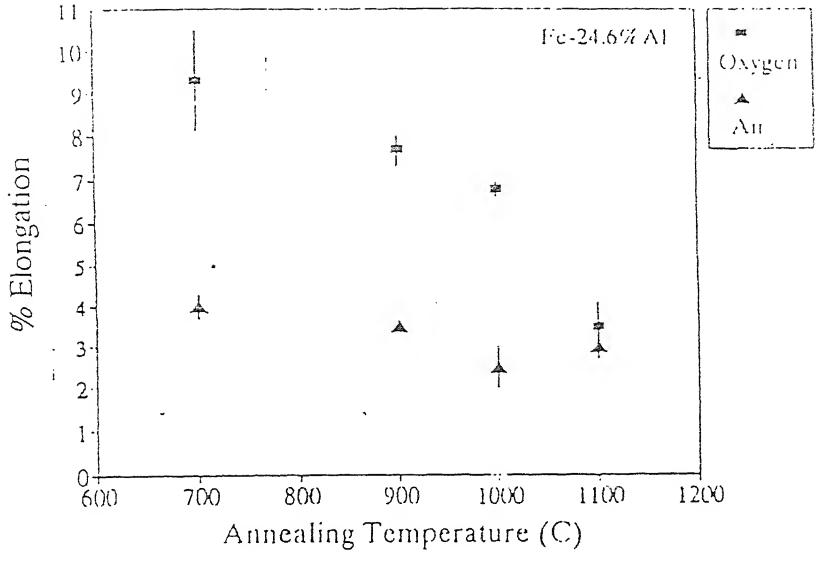

Figure 6. Elongation versus annealing temperature for Fe-24.6Al tested in oxygen and laboratory air [25].

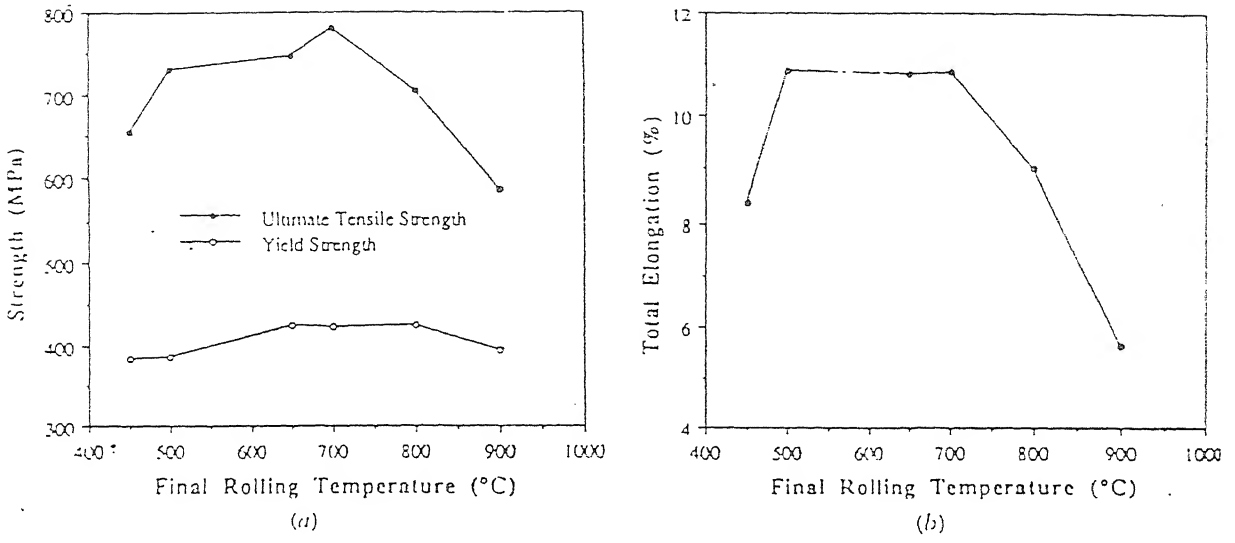

Figure 7. Tensile properties obtained from various processing temperatures (a) yield and ultimate tensile strength and (b) tensile elongation [29].

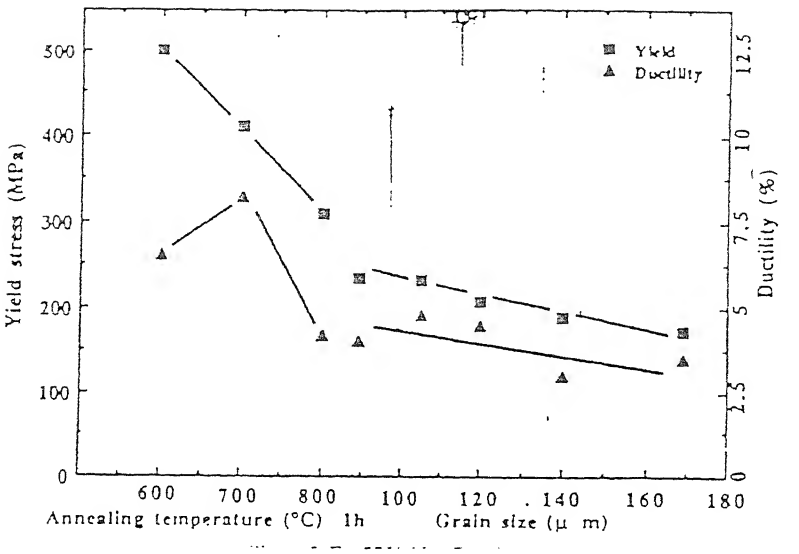

Figure 8. Yield stress and tensile ductility of Fe-28Al-4Cr alloy after annealing to recovery or recrystallization [26].

annealing at 700^{0}C by Morris and Leboeuf in Fe-28Al-4Cr [26]. It is interesting to note that B additions to iron aluminide increases the recrystallisation temperature and reduces the recrystallised grain size in FeAl alloys, thereby retaining the hardness at room temperatures when provided a comparative anneal as base iron aluminide (Figure 9 and 10 [28]).

The B2 structure, when compared to the DO_3 structure, is beneficial to the mechanical properties at room temperature, by essentially changing the fracture mode [27]. Heat treatment can effectively produce the phase that is required and hence it can affect the tensile properties of iron aluminides. A heat treatment to produce mixed B2 + DO_3 structure or B2 structure with complete recrystallisation results in low tensile properties whereas the B2 treatment + no recrystallisation results in a higher fracture strength and ductility in Fe-28Al-5Cr-O.3B-O.003Mg alloy (Figure 11). This figure also shows that grain boundary strength in unrecrystallised + B2 structure is higher than that of cleavage strength, thereby resulting in higher ductility. However, with a fully recrystallised structure, both the grain boundary and cleavage strength are lower than that for partially recrystallised structure resulting in rather poor ductilities in this condition.

Heat treatments also affect fracture toughness of iron aluminides. The fracture toughness, K_{IC}, the threshold value of stress corrosion cracking, K_{ISCC}, and threshold value of hydrogen induced cracking K_{IH} of Fe-28Al-5Cr are presented in Table 4 [34].

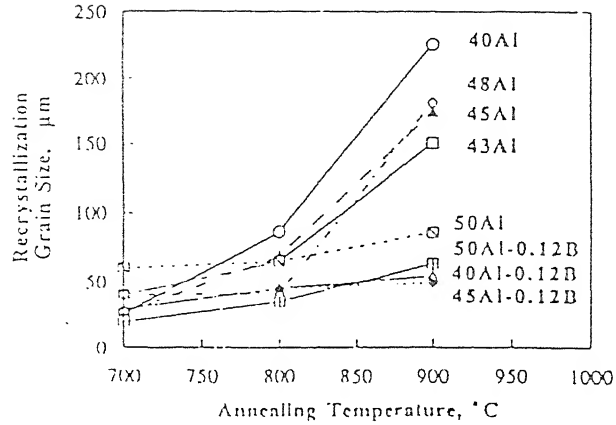

Figure 9. Grain size in the recrystallized zone versus annealing temperature for Fe-Al alloys [28].

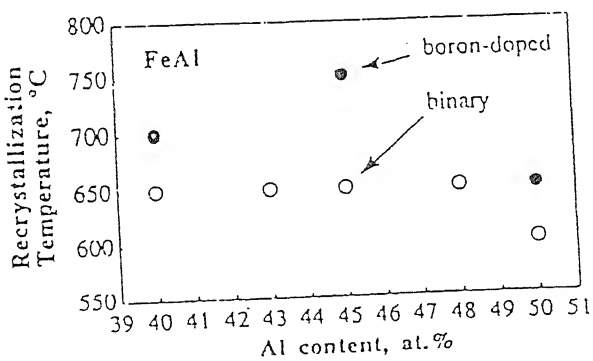

Figure 10. Effect of boron on the recrystallization temperature [28].

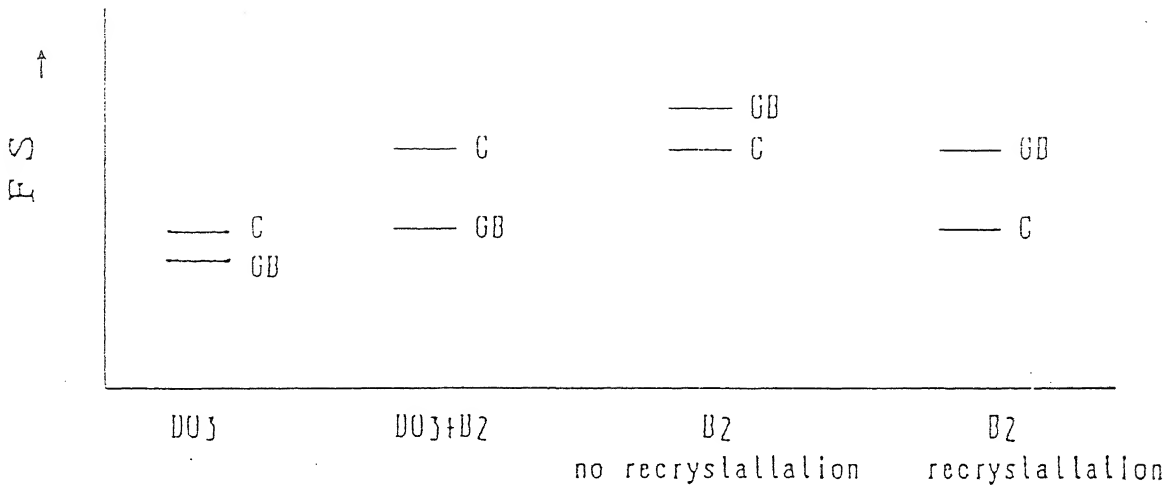

Figure 11. Schematic showing the effect of heat treatments on fracture strength (FS) of Fe-25Al-5Cr-0.3B-0.003Mg [27].

Table 4 the K_{IC}, K_{ISCC} and K_{IH} of Fe_3Al + Cr

Specimens	K_{IC} ($MPam^{1/2}$)	K_{ISCC} ($MPam^{1/2}$)	K_{IH} ($MPam^{1/2}$)
Treatment A Annealed 700^{0}C 2hrs	30.1	16.1	10.1
Treatment B Annealed 900^{0}C 1hr and 700^{0}C 2hrs	32.2	19.2	13.2

It can be seen that the K_{IC}, K_{ISCC}, and K_{IH} of the specimen with unrecrystallised structure is lower than that with a completely recrystallised structure, the reason for this behaviour is not yet clear. It was also observed that cleavage fracture occurred easily in ordered alloy with unrecrystallised structure implying that the unrecrystallised structure restricts the occurrence of intergrannular fracture. This has been attributed to the higher dislocation density for specimen after treatment. A than after treatment B (Table 4), which results in a large capacity of grain interior to trap hydrogen. Therefore, the difference in hydrogen content between the grain boundary and the grain interior is small which facilitated the occurrence of the cleavage fracture [34]. Therefore, it has been proposed that the unrecrystallised structure restricts the occurrence of intergrannular fracture.

Lynch [25] has shown that TMP (thermomechanical processing) results in ductility enhancement which is independent of the type of environment used for testing implying that TMP increases the intrinsic ductility of iron aluminide rather than decreasing its susceptibility to embrittlement. Lynch has shown that grain boundaries are not necessary for moisture induced embrittlement of iron aluminide and TMP effects are not controlled by grain boundaries. However, the cause of this effect is still

unknown. The intrinsic ductility increase caused by the TMP effect is likely due to changes in dislocation behaviour and/or the disordering of material.

2.4.1 MECHANISM FOR HYDROGEN EMBRITTLEMENT MINIMIZATION

The exact mechanism of minimizing the embrittlement by controlling the microstructure is yet unresolved. One of the mechanisms suggests that the elongated grain structure characteristics of as-rolled and partially recrystallised structure provides a minimum of transverse cleavage planes as well as minimum of grain boundary area. This suppress the atomic hydrogen ingress and also the grain boundary diffusion of hydrogen is reduced. Therefore, the extent of hydrogen embrittlement is also reduced[15]. However it is difficult to imagine that the diffusivity of hydrogen would be very much different in grain boundary and bulk regions of iron aluminides and therefore the results for ductility enhancement in case of partially recrystallised microstructure could also be due to some other reasons. It has been hypothesized that HE is minimum for the partially recrystallized structure due to the unrecrystallised structure disrupting the diffusion of hydrogen [15]. This may not be the reason as hydrogen can diffuse with relative ease in iron aluminide matrix and grain boundaries. The hypothesis has been ruled out by the fact that, if grain boundaries play an active role in the environmental embrittlement of iron aluminides, then the single crystals should be very resistant to embrittlement. However, the single crystals of iron aluminides are susceptible to embattlement like polycrystals [25], indicating that the presence of hydrogen within the grain is responsible for embrittlement.

A possible reason for enhancement of ductility due to partially recrystallised structure would be the reduction in dislocation density during stress relief annealing

treatment [11]. The gliding a<111> dislocations in Fe_3Al are composed of two a/2 <111> partials joined by an antiphase boundary [31]. Hydrogen is transported primarily to these partial dislocations deep down into the material. Further the partial dislocation are locked as immobile <100> dislocations and twice the normal amount of hydrogen can be absorbed by these locked dislocation [35]. According to all theories of hydrogen embattlement, the concentration of hydrogen should exceed a critical amount to cause embattlement and this critical concentration is achieved in (100) planes due to above reasons [15, 35]. Once the critical concentration is achieved, hydrogen causes decohesion of the matrix and this is verified by cleavage fracture observed in this class of iron aluminide [36]. Moreover, etch-pit studies have shown that the cleavage facets are of (100) type [10], further confirming the above mechanisms. This improvement in ductility upon stress relieving the micro structure could be due to the reduction in number of a/2<111> dislocation in the structure during the annealing treatment with a lower amount of a/2<111> partials in the microstructure; the local accumulation of hydrogen and locking partials could be less severe and hence this would result in an enhanced ductility as observed experimentally [2, 10].

Another hypothesis [26] suggests that the dislocations present at subgrain boundaries are of burger vector 1/2<100> [26]. This results due to room temperature heavy deformation, according to association of partials

$$1/4\,[111] + 1/4\,[111] \rightarrow 1/2\,[100]$$

This dislocation of burger vector 1/2 [100] are likely to remain immobile during subsequent deformation of the relaxed material since this has been never been identified as taking part in the deformation of Fe_3Al alloy. As such, the subgrain boundaries are strong obstacles to deformation at room temperature estimates of

bowing stress required for a glissile dislocation to pass through the boundary network by an orowan type mechanism or taking account of forest intersections mechanism confirms this. At the same time the subgrain boundaries will not be dissociated or destroyed by the passage of glissile dislocations; it will remain as an obstacle avoiding the concentration of stress or strain inside the material. For this reason the fracture mechanism by stress or strain concentration at grain boundaries or piles up will be retarded, thereby increasing the ductility [26]. Thus, mild annealing of cold worked Fe_3Al based alloys can lead to good ductility combined with strength when annealing treatment leads to dislocation recovery into a subgrain structure rather than leading to complete recrystallisation. This behaviour arises because of the glissile <111> type dislocation present after deformation have reacted in subgrain walls to produce stable network containing mostly <100> type dislocations. The subgrain walls are strong barrier to dislocation movement and thus retain considerable strengthening and are stable during plastic deformation such that the creation of intense local stress or strain concentrations, leading eventually to failure is retarded. Additional research focused on the effects of dislocations are necessary to understand the cause of TMP effects.

There is a sacrifice in strength upon the recrystallisation treatment. Complete recrystallisation will lead to a large decrease in strength [15] and therefore not a viable alternative. The exception to the above would be when the alloying additions produces a fine grain size after recrystallisation annealing in which the strength would not decrease drastically. Interestingly Ce additions [22] and Mm additions [23] to iron aluminides produces a fine grained recrystallised structure unlike the large grain obtained for iron aluminide without Ce additions and there is no degradation of strength for the Ce alloyed iron aluminides even in the recrystallised condition. Boron

is also a promising prospective as the grain sizes are lower with B addition after recystallisation [19, 20, 28]. Moreover, the addition of Zr also results in increased ductilities, the reason for which has been proposed to be the partially recrystallised microstructure which the addition leads to [15]. Therefore the addition of elements to inhibit recrystallisation would also be beneficial in improving the room temperature ductility of iron aluminide.

2.5 DIFFUSIVITY OF HYDROGEN IN METALS

The recent increase of experimental work on diffusion of hydrogen in metals has been motivated from the view point of genuine understanding of many peculiar features of hydrogen diffusion in metals including the magnitude of diffusion coefficient, their dependence on temperature and crystal structure and interaction of hydrogen with dislocation and traps.

A high jump rate (typically 10^{12} jumps per second) together with a low activation energy for hydrogen bulk diffusion (typically 100 meV), high mobility of hydrogen and its isotopes (D, T, μ^-) [38, 39] are the origin of long range diffusion and hydrogen embrittlement in metals. At a given temperature the diffusion of hydrogen occurs orders of magnitude faster than those of other interstitially dissolved elements such as oxygen nitrogen and carbon.

Figure 12 [38] shows a comparison for H, O and N diffusion in Nb and for C in Fe. Phenomenologically, this low diffusivity is a consequence of low activation energy for hydrogen diffusion. In interstitial diffusion, interstitials have to move from one interstitial to another. In this process, the interstitial has to force the parent atoms apart in order to move to next interstitial site. As the size of hydrogen atom is smaller than

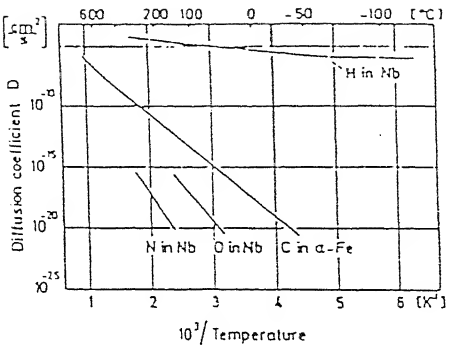

Figure 12. Diffusion coefficients of H, N and O in Nb and C in α-Fe [38].

the other interstitials, it can move easily from one interstitial to another, which is reflected in the low activation energy for hydrogen diffusion.

2.5.1 INFLUENCE OF CRYSTAL STRUCTURE

It has been shown by several reserchers [38, 39] that the transition from a closed packed to a BCC structure leads to a drastic increase of the diffusion coefficient, caused by a decrease in the activation energy. The activation energy for hydrogen diffusion in γ-iron is 0.5 eV, while that in α-iron is 0.05 eV to 0.1 eV, i.e. a change of an order of magnitude in hydrogen diffusion coefficient for transtion FCC$\rightarrow$BCC. In case of titanium, activation energy for H diffusion in β (BCC) is 0.29 eV while that in α (HCP) is 0.54 eV [38].

This higher diffusivity is attributed to the less closed packed structure of the BCC structure. In the FCC structure, there is one octahydral site per host atom, whereas in BCC structures, three octahedral or six tetrahedral sites are present per host atom. If d is the nearest neighbour distance, the average distance of the interstitial sites is d in FCC and $d/\sqrt{3}$ or $d/\sqrt{6}$ in BCC structures, respectively. The smaller nearest neighbour distance in BCC suggest that the activation barrier is smaller or that the tunnelling of hydrogen can be easier.

No literature was found on the influence of ordered structure and the degree of ordering on the hydrogen diffusivity in iron aluminides. However, hydrogen diffusion can be related to diffusion of boron in iron aluminide as boron is neither strictly interstitial nor substitutional solute. It has been shown that the diffusion of boron is faster in the disordered state than in the ordered state and moreover, diffusion of boron

is much faster in the B2 ordered structure of Fe_3Al than the DO3 ordered structure [40]. The data provided is

Do B = 8.7×10^{-6} cm^2/s at 1013K - 823K (B2)

Do B = 2.6×10^{-13} cm^2/s at 803K - 623K (DO3)

Similar results were obtained for the diffusion of substitutional elements nickel, vanadium and titanium in Fe-26 at% Al in which the atomic arrangement changes from disordered state to the B2 ordered state at 1023K, and from the B2 ordered state to

DO3 ordered state at 823K [41]

Do Ni = 5.8×10^{-5} cm^2/s at 1055K - 839K (B2)

Do Ni = 0.9×10^{-12} cm^2/s at 816K - 722K (DO3)

Do Ti = 1.4×10^{-6} cm^2/s at 1013K - 823K (B2)

Do Ti = 1.8×10^{-12} cm^2/s at 823K - 623K (DO3)

Do V = 1.8×10^{-6} cm^2/s at 1013K - 823K (B2)

Do V = 1.5×10^{-12} cm^2/s at 823K - 623K (B2)

It must be again noted that the diffusivity of these elements in the DO3 structure is drastically reduced compared to the B2 structure. Moreover, Bernardini *et al* [42] reported that the volume diffusion coefficient of iron in iron aluminide increases with temperature as the structure in Fe-24.6Al changes from DO3 (ordered) to partially disordered B2 and then further at high temperature to the completely disordered A2 structure. Thus, it is clear that the diffusion is enhanced in the following transition DO3 (Ordered) $\rightarrow$ B2 (Ordered) $\rightarrow$ A2 (Disordered).

Based on the above considerations, it can be concluded that hydrogen diffuses slower in the ordered structure and hydrogen diffusivity decreases as the degree of ordering increases.

2.5.2 EFFECT OF TEMPERATURE ON HYDROGEN DIFFUSION

Hydrogen diffusivity in α-Fe always increases with temperature [43]. Kiuchi and McLellen [43] have analyzed the published hydrogen diffisuvity data in α-Fe and have noted that there is a large scatter in the values of hydrogen diffusivity in iron obtained, particularly at low temperature. They emphasized that this large scatter at low temperature is due to various trapping effects of hydrogen, which are more effective at lower temperature or virtually irreversible at low temperature while at high temperature thermal detrapping dominates. They have critically analyzed the data based on the method that was used to determine the diffusivity and have provided the best representation of hydrogen diffusivity in α-Fe as [43]

$D = 7.23 \times 10^{-B} \exp(-Q/RT)\ m^2/s$ (-40^0C to 80^0C)

where Q = 5.69 kJ/mol

and in the temperature range the best D representation is given by [43]

$D = (1 \text{ to } 2.52) \times 10^{-7} \exp(-Q/RT)\ m^2/s$ (50^0C to 550^0C)

where Q = 6.70 to 7.12 kJ/mol

They pointed out that with increasing temperature, the fraction of hydrogen atoms hopping from octahedral sites increases rather than tetrahedral sites and this is the reason for the higher activation energy obtained at higher temperatures.

Nagano *et al* [44] have studied the intrinsic diffusivity of hydrogen in α-Fe in a wide temperature range (290K-1040K). This intrinsic diffusivity was free from surface effects and trapping effects (explained in the next section) and was exclusively dependent on temperature. The temperature dependence of diffusivity of hydrogen in α-iron is shown in Figure 13 [44]. The higher diffusivity of hydrogen at higher temperatures is attributed to the lower activation energy for diffusion because the

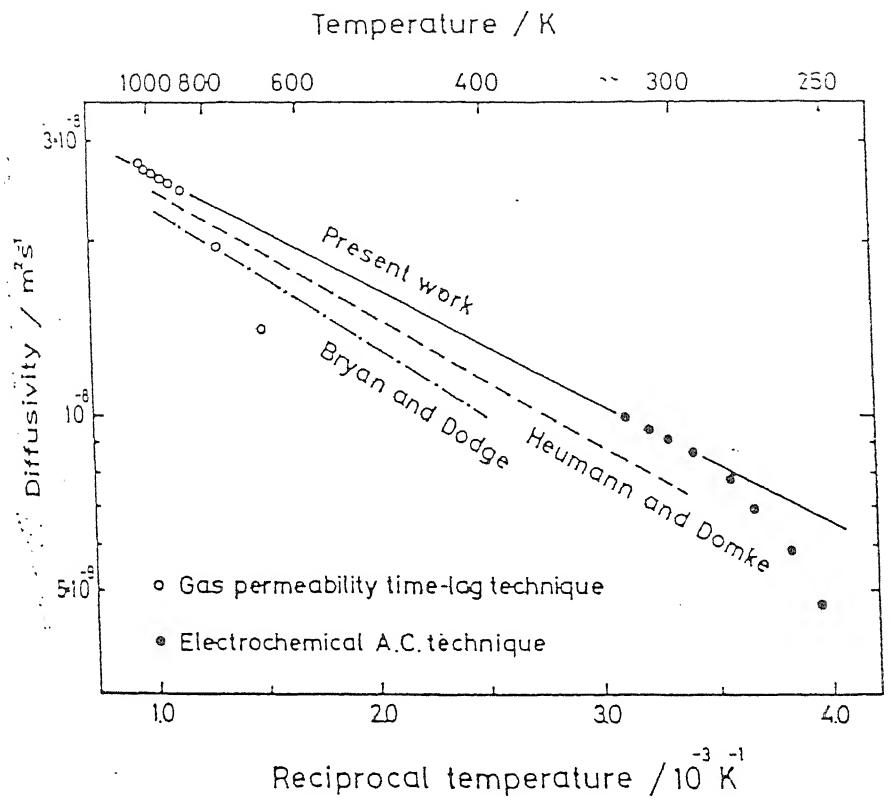

Figure 13. Temperature dependence of hydrogen diffusivity in α-iron [44].

atoms at high temperature are in vibrational state and hence the hydrogen can easily be tunneled through. However, this intrinsic diffusivity at higher temperature can be affected by surface effects such as surface inhibition reaction and/or surface oxide films, as well as trapping effects (loss effective) and this may reduce the intrinsic hydrogen diffusion coefficient. Secondly, at higher temperatures the hydrogen atoms which are inside the traps can easily get out of the trap due to thermal energy. At lower temperatures it is not easy for hydrogen to get out of the trap because thermal energy is not sufficiently higher than the binding energy of trap. At low temperature, equilibrium between hydrogen concentration in trap and the lattice exists. Therefore, at low temperatures, diffusion of hydrogen not only requires energy to diffuse through lattice but also requires some extra energy(= binding energy of trap) to overcome the trap and hence activation energy for diffusion at low temperature increase. Figure 14 [45] shows the effect of temperature on hydrogen diffusivity in α-Fe. This shows that E_O the migrational energy, at high temperatures is 7 kJ/mol while at low temperatures, it is 35 kJ/mol. In this Figure, T_A is the temperature high enough for adequate diffusion of hydrogen and T_B is temperature low enough for hydrogen trap bonding energy E_B to dictate a significant population of hydrogen in trap sites that lead to embrittelment.

Therefore, the interaction of hydrogen with trapping sites affects the diffusivity of hydrogen and this aspect would be reviewed in the next section.

2.5.3 HYDROGEN TRAP INTERACTION

A single hydrogen trap interaction occurs by a reaction of type

$$H + T = H_T$$

Where H is hydrogen in the lattice, T is the trap and H_T is hydrogen that is bound to the trap. The escape of hydrogen from the trap can be represented by

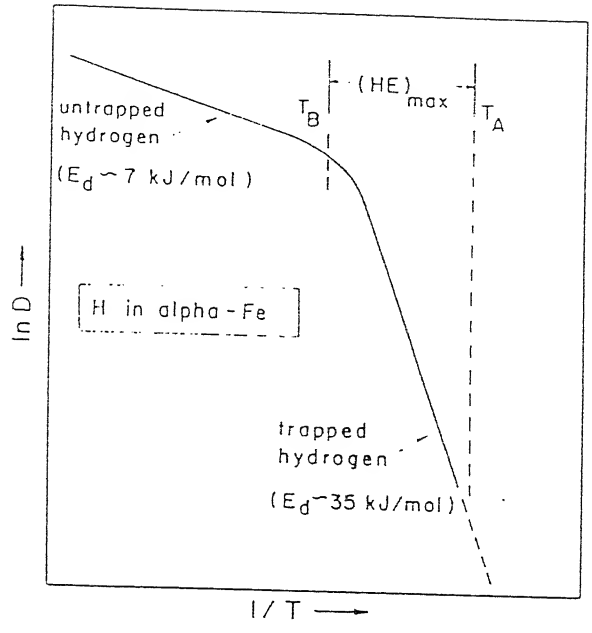

Figure 14. Schematic illustration of diffusivity of hydrogen in α-iron. Room temperature typically falls in the range between T_A and T_B where apparent migrational energy Ed is high [45].

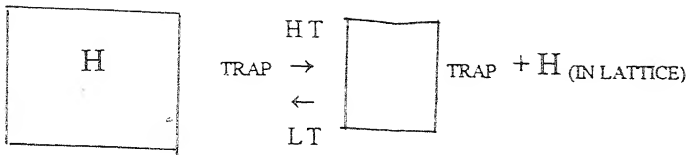

where  TRAP is a trapping site and HT and LT are high temperature and low temperature, respectively.

Troiono *et al* [46] were among the first investigators to recognize the importance of hydrogen in solution causing hydrogen embrittlement and that hydrogen trap interactions had to be large enough to play a critical role in the embrittlement. It is generally accepted that significant hydrogen trap interactions are a rule rather than exceptions. Impressive progress has been made to relate specific hydrogen trap interactions to hydrogen embrittlement [45, 47-49]. When a hydrogen atom jumps from a normal lattice site into a trap, the probability of an eventual return to the former site is decreased. In some cases, small very probable jump increments are needed to get out of the trap while in other cases only one less probable and may be impossible jump is required to get out of the trap, making the trap irreversible. The energy required for H atom to get out of the trap is called binding energy of the trap E_B.

The attractive force for hydrogen to get into the trap are of four types viz. electrical fields, stress fields, temperature gradients and chemical potential gradient [50]. As a hydrogen atom dissolves in transition metals by giving up its excess electrons to the collective electron gas of the metal, any defect that introduces an electron vacancy will attract hydrogen to achieve local neutrality. This will be the case for impurities on the left of the matrix element in the periodic table. This is a typical example of electrical force. The second type of force owes its origin to tensile stress fields induced by defects such as dislocations, coherent and semi coherent grain

boundaries, particles and crack tips. Since the solubility of hydrogen increases with temperature, attractive forces will be developed by thermal gradients whenever the heterogeneous temperature distribution will exists. The last force that is the chemical potential gradient is thermodynamical in nature for example, activity coefficient a_H of hydrogen in steel may be expressed as

$\varepsilon_H^i i = \varepsilon \ln(\gamma_H) = \ln(\gamma_H^o) + \Sigma \varepsilon_H^i X_i$. An attractive force between i and H will exist whenever ε_H^i is negative [50].

There are some other physical traps, in which the diffusing hydrogen atom will randomly fall into this trap such as microvoids, vacancies and cirmumferential microcracks along particle matrix interface.

Hydrogen traps can, therefore, be classified as both attractive traps as well as physical traps and each trap will have its binding energy E_B which must be overcome for the further diffusion of hydrogen. E_B, the binding energy of trap and its relation to other thermodynamic parameters that characterize hydrogen in iron are given in Figure 15 [45]. If E_S is the heat of solution of hydrogen in iron (= 29 kJ/mol [45]), we can define a trap as weak if $E_B < E_S$, of moderate strength if $E_B = E_S$ and strong if $E_B > E_S$. Traps with E_B of this magnitude are not drained of hydrogen by thermal detrapping at temperature in the vicinity of room temperature and such traps have high saturabilities and are present in largest densities in the more microstructurally complicated high strength steels which are most susceptible to hydrogen embrittlement. Traps are also differentiated on the basis of binding energy E_B to the migrational energy E_m as reversible $E_B = E_m$ and irreversible if $E_B > E_m$. D. A. Johns has [51] sumarized the

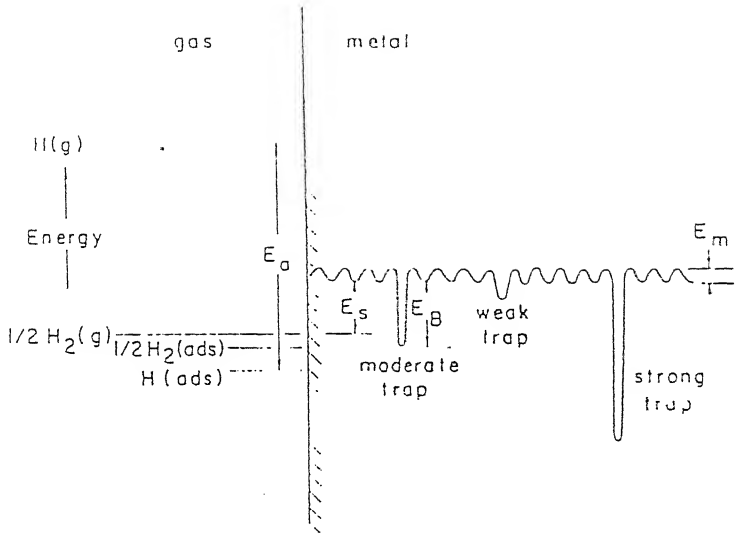

Figure 15. Potential energy diagram for hydrogen in gas and solid states in α-iron. Ea is the energy of adsorption and Em is the lattice migrational energy of hydrogen in iron. Note that Em ~ Ed ~ 7 KJ/mol at $T>T_B$ and that Ea ~ E_B for strong traps [45].

various traps present in the iron. It has been reported that for embrittlement to occur, the hydrogen concentration should be above a critical value at the sites of high stress concentrations. For embrittlement, the hydrogen should be able to reach the high stress concentration sites during straining in sufficient quantity (above the critical concentration) from its trapping sites. Hydrogen bonded to irreversible sites are immobile and act only as sink and not as a source of hydrogen, hence does not contribute to embrittlement, while reversible traps act as sink as well as source of hydrogen and hence can aid embrittlement. Thus, irreversible hydrogen traps plays a dominant role in improving hydrogen embrittlement of metals.

It is therefore evident that the traps play an important role in the hydrogen embrittlement. A microstructure consisting of an uniform fine distribution of strong hydrogen traps should maximise an alloys resistance to hydrogen. Therefore, if one has to design alloys exhibiting such a microstructure the need arises to know what kind of traps should be used.

2.5.3.1 TYPES OF MICROSTRUCTURAL TRAPS FOR HYDROGEN

The various types of microstructural traps for hydrogen can be classified as follows [51]

i) Interstitials: Interstitials (like C and N) present in iron acts as weak traps having a binding energy E_B = 15 kJ/mol. Such type of traps are reversible in nature and they act as sink as well as source of hydrogen [52].

ii) Substitutional Atoms: Pressouyre and Bernstain [53] studied the diffusion of hydrogen at room temperature in relatively pure iron containing small differing amounts of titanium (0.15 to 1.5 wt%Ti). They obtained a linear relationship between the diffusivity ratio with and without titanium in iron, and the number of titanium traps

(equal to the number of titanium atoms). They have shown that the titanium atoms are potential trap sites and about 100 hydrogen atoms cluster around each Ti atom. The traps were reversible in nature with a binding energy (E_H^{Ti}) of 27 kJ/mol. Troiano [46] mentions that Ti atoms in steel act as moderate traps with E_B = 20 kJ/mol. It is to be noted that Ti is a strong hydride former while the rest of the substitutional atoms in steel have binding energy less than that of titanium [52].

In the case of aluminides, Gleason *et al* [54] suggest that hydrogen interacts strongly with the transition-metal component of the aluminides. According to them, the desorption of H_2O from FeAl occurs at temperatures near 27^0C and the hydrogen product from the decomposition of water desorbs at about 227^0C. This is the hydrogen that is trapped in the lattice and also from the surface regions.

iii) Vacancy, Microvoids and Cracks: These metallurgical defects are incorporated into the metals due to excessive cold working and/or wrong heat treatment. Choo and Lee [55] have studied the effect of cold working on hydrogen diffusivity in iron and they obtained a hydrogen release peak as a shown in the Figure 16 [55]. This figure clearly shows that the hydrogen release peak is maximum for iron of lower relative density (obtained by cold working) compared to iron of higher relative density. This provides the evidence that microvoids act as hydrogen traps. Yang *et al* [56] have also confirmed this fact. They studied the absorption and desorption of hydrogen in B2 Fe-40Al. When they heated the hydrogen diffused sample in the intermediate temperature of about 500^0C-600^0C, they obtained a hydrogen release peak due to hydrogen trapping at vacancies (i.e. P_i) as shown in the Figure 17 [56]. The above result was in confirmity with the fact that the retained vacancies are eliminated by heat treatment around temperature 400^0C. As vacancies are stable sites for hydrogen trapping,

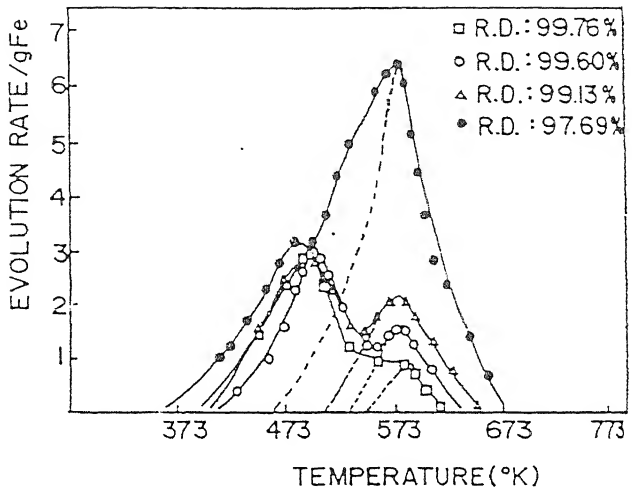

Figure 16. Dependence of height of peaks on the amount of microvoids [55].

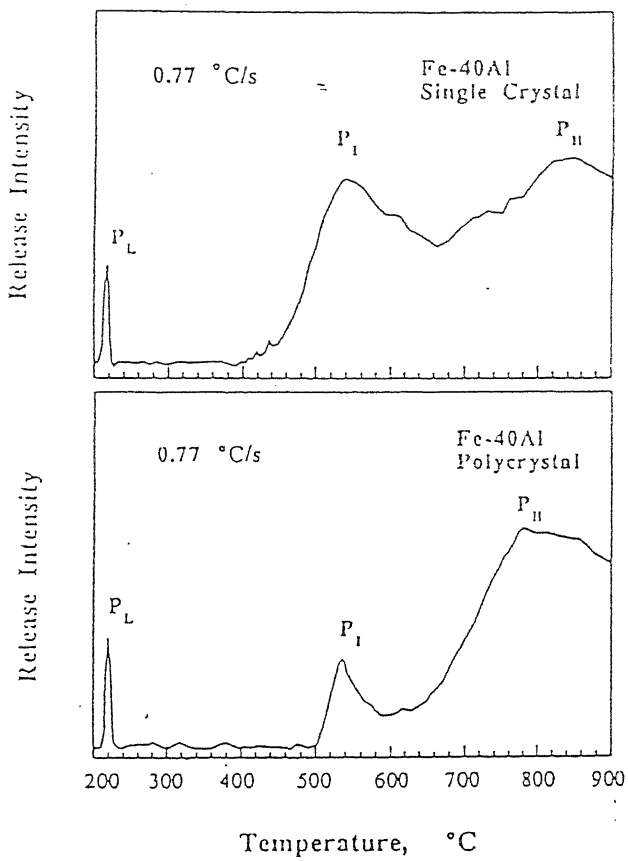

Figure 17. Hydrogen release intensity as a function of temperature [56].

hydrogen was released when vacancies were removed. They also found out that hydrogen trapped at the grain boundaries (provided by the release peak P_H) possessed a higher stability than in a vacancy. The hydrogen in the lattice (i.e. peak P_L) possessed the least stability.

iv) Matrix-Precipitate Interfaces: In order to study the influence of oxide/metal interface on hydrogen trapping, Huang *et al* [57] studied the hydrogen behaviour in Pd-Al_2O_3, Pd-MgO, Pd-ZnO, Pd-ZrO_2 alloys prepared by internal oxidation technique. The trapping of hydrogen at the interfaces was also indirectly confirmed by Govind *et al* [58] in the Cu-Al_2O_3 system also prepared by internal oxidation. Huang *et al* [57] found that all alloys exhibited a strong tendency for hydrogen trapping. They showed that internal oxidation in air leaves excess oxygen at the interfaces that is not bound in the same way as oxygen within the oxide. The strong irreversible trapping of hydrogen, in these system, was related to this excess oxygen at the interfaces, which form O-H bonds. Their experiments also suggested hydrogen trapping in the stress fields around the precipitates and this trapping was maximum near the matrix-oxide interface. Similarly, Pressoure *et al* [50] found that TiC in α-Fe acts as an irreversible hydrogen trap.

v) Grain Boundaries: Kirchein [59] has studied the effect of grain boundaries on hydrogen diffusion in nanocrystalline Pd of average diameter 1 μm. Hydrogen diffusivity increased remarkably as compared to that in a normal polycrystalline sample of average grain diameter 20 μm. This was due to increase in volume fraction of grain boundaries by several orders of magnitude in a nanocrystalline material as compared to polycrystalline material. There was increase in solubility of hydrogen by a factor of 10 to 30 in nanocrystalline material while the concentrations of hydrogen within the grains

was same in both the materials. These results indicate that grain boundaries may act as reversible traps. Choo and Lee [55] have shown for pure iron that hydrogen diffusivity increased as the ASTM grain size number increases from 2 to 9 (Figure 18) [55]. The maximum hydrogen solubility was obtained for iron with grain size no 9 and least hydrogen solubility was obtained for iron with grain size no 2.

Therefore, grain boundaries act as condensation sites for hydrogen. Yang *et al* [56] also confirmed this in Fe-20Al as they correlated the hydrogen largest hydrogen release peak in B2 Fe 40Al during the hydrogen desorption at higher temperature to be due to hydrogen trapped at grain boundaries (Figure 17).

vi) Dislocations: Dislocations are suggested to be principle trap sites among above mentioned traps and its interaction with hydrogen has been studied rather extensively [60-63].

Many researchers have agreed that hydrogen is trapped at the dislocations and it is often observed that hydrogen is transported by dislocation motion and both the dislocation arrangement and stress fields of dislocations plays important role in hydrogen trapping.

Kumnick *et al* [61] insisted that hydrogen is trapped not at the stress field of dislocation but at the long range field of dislocation debris. However, Hong [60] has shown that the hydrogen is trapped at the stress field of dislocation and not at the core of each dislocation. He found that the amount of hydrogen trapped is small in cold worked state than in the annealed state. He suggested that in the cold worked state stress field of each dislocations are overlapped as dislocations are densely tangled and then the area affected by stress fields of dislocation is very small, while in the annealed state, the densely tangled dislocation are loosened and stress affected region is

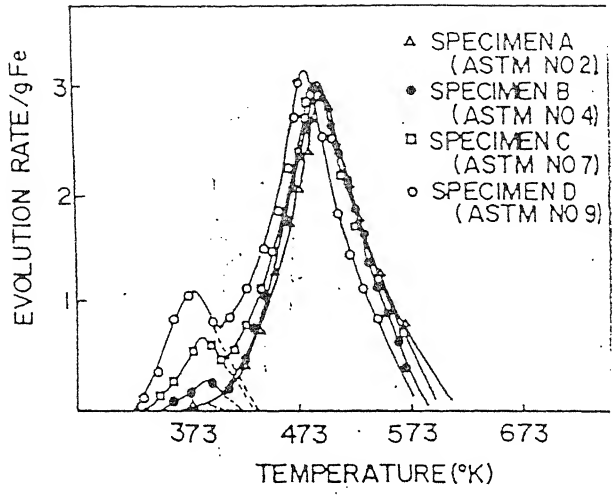

Figure 18. Dependence of height of peaks on the amount of grain boundary area [55].

increased because stress field of each dislocation acts separately, so the amount of hydrogen trapped increases.

The second interesting aspect of hydrogen dislocation-interaction is that hydrogen increases dislocation mobility. Hydrogen promotes the nucleation rate of kink by lowering the activation energy of formation between dislocation and kink, and the dislocation mobility increases especially when the hydrogen escapes from a dislocation to a normal lattice site [63]. Firm evidences for the enhancement of dislocation mobilities in the presence of hydrogen has been provided by Birnbaum and co-workers using tensile stage transmission electron microscopy in an environment chamber [62].

Dislocations are also termed as mixed trap (attractive traps+physical trap): the attractive character is due to mechanical forces induced by stress fields and the physical character is due to tensile region of core where lattice is distorted [50]. There are several aspects that still need to be understood like the acceleration mechanisms of hydrogen on dislocation motion and the effect of dislocation structure on trapping behaviour.

vii) Surface traps: Kiuchi and McLellan [43] in their over view on hydrogen diffusivity in α-Fe had noted that the scatter in the diffusivity was maximum around room temperature, which they attributed to surface trapping effects. They reported that inappropriate surface finish or mechanical abrasion produces thin "Bielby" layers containing microvoids and a high amount of dislocations which act as a surface trapping sites and which cannot be removed by annealing. This thin "Bielby" layers have maximum hydrogen solubility. They then emphasised the fact that electropolishing and palladium coating the specimens before the experiments can

obviate surface trapping effects. They concluded that the diffusion coefficients obtained under electropolished conditions (+Pd coated) are more reliable. Palladium coating ensures reproducible hydrogen entry conditions as Pd acts like a "spill-over".

If the surface is not electropolished and palladium coated, the deformed layers present on the surface act as surface traps and the total area available for diffusion decreases with time as surface trapping increases. The surface trapping effect also stems from another effect. These surface layers contains oxygen as the oxygen penetration into the grain boundaries cannot be prevented even under ultra high vacuum and this oxygen acts as a inhibitor for hydrogen towards grain boundary migration and this H-O interaction increases hydrogen solubility, but electropolishing can obviate this problem.

2.6 HYDROGEN DIFFUSION IN IRON ALUMINIDES

The pronounced susceptibility of iron aluminides to hydrogen embrittlement may be a consequence of ordering effects on diffusion behaviour or of an enhanced fracture mechanism. Long range order generally is considered to slow the diffusion. However, extensive experimental data on room temperature diffusivity of hydrogen in iron aluminides is lacking. It has been already reviewed in section 2.2 that cracking caused in iron aluminides is due to hydrogen. The following sub-sections review the entry and diffusivity of hydrogen in iron aluminides with a short introduction on the diffusivity of hydrogen in Fe and Al. As regards diffusivity of hydrogen in pure Al and α-Fe, there are several published reports that are available. The topic of hydrogen diffusion in pure α-Fe has been reviewed by Volkl and Alefeld [39, 39] and by Kiuchi and McLellan [43]. Fig. 19 [38] and Fig. 20 [43] show the values of diffusion coefficient of H in α-Fe obtained by various researchers. The interesting feature that is

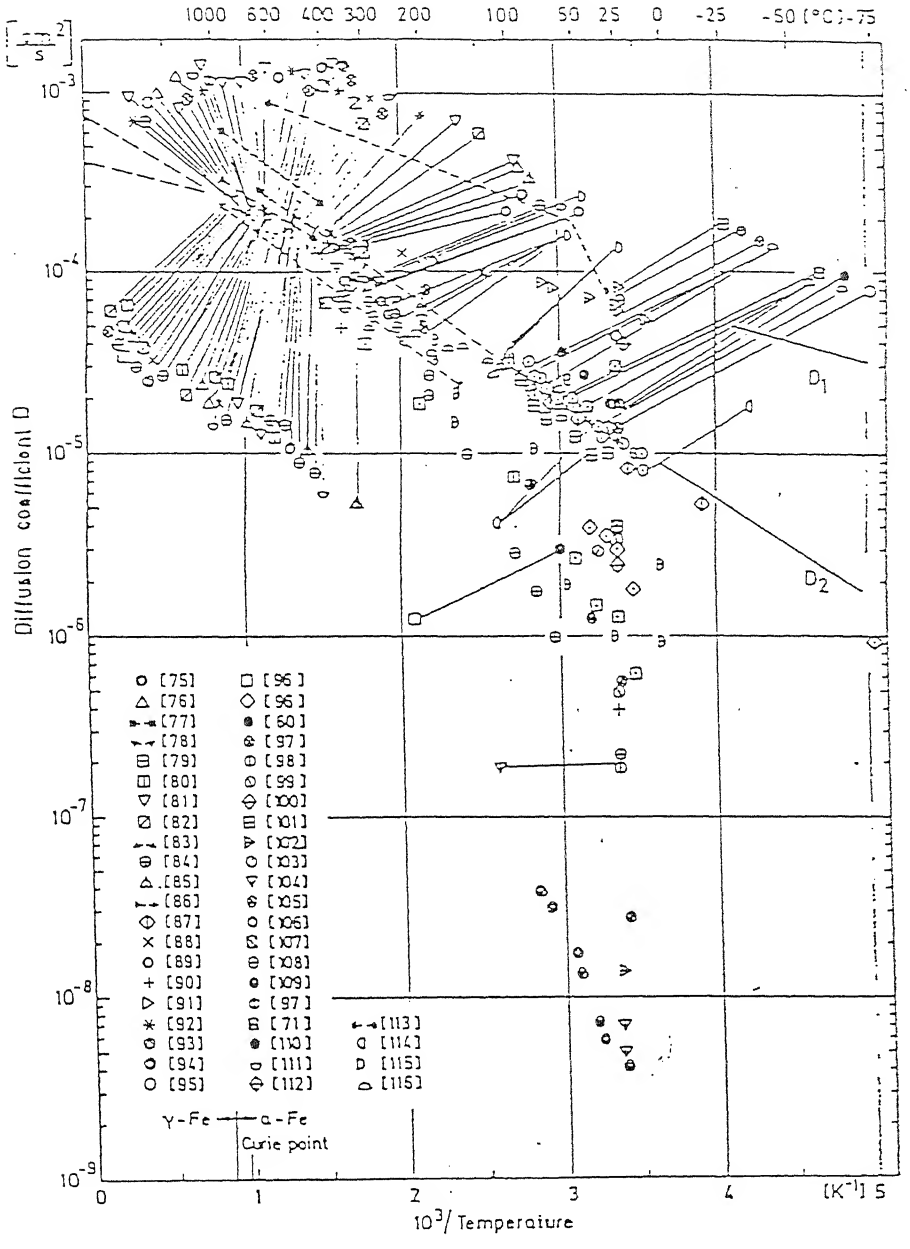

Figure 19. Diffusivity of hydrogen in α-Fe. Number in brackets refer to literature cited in reference [43].

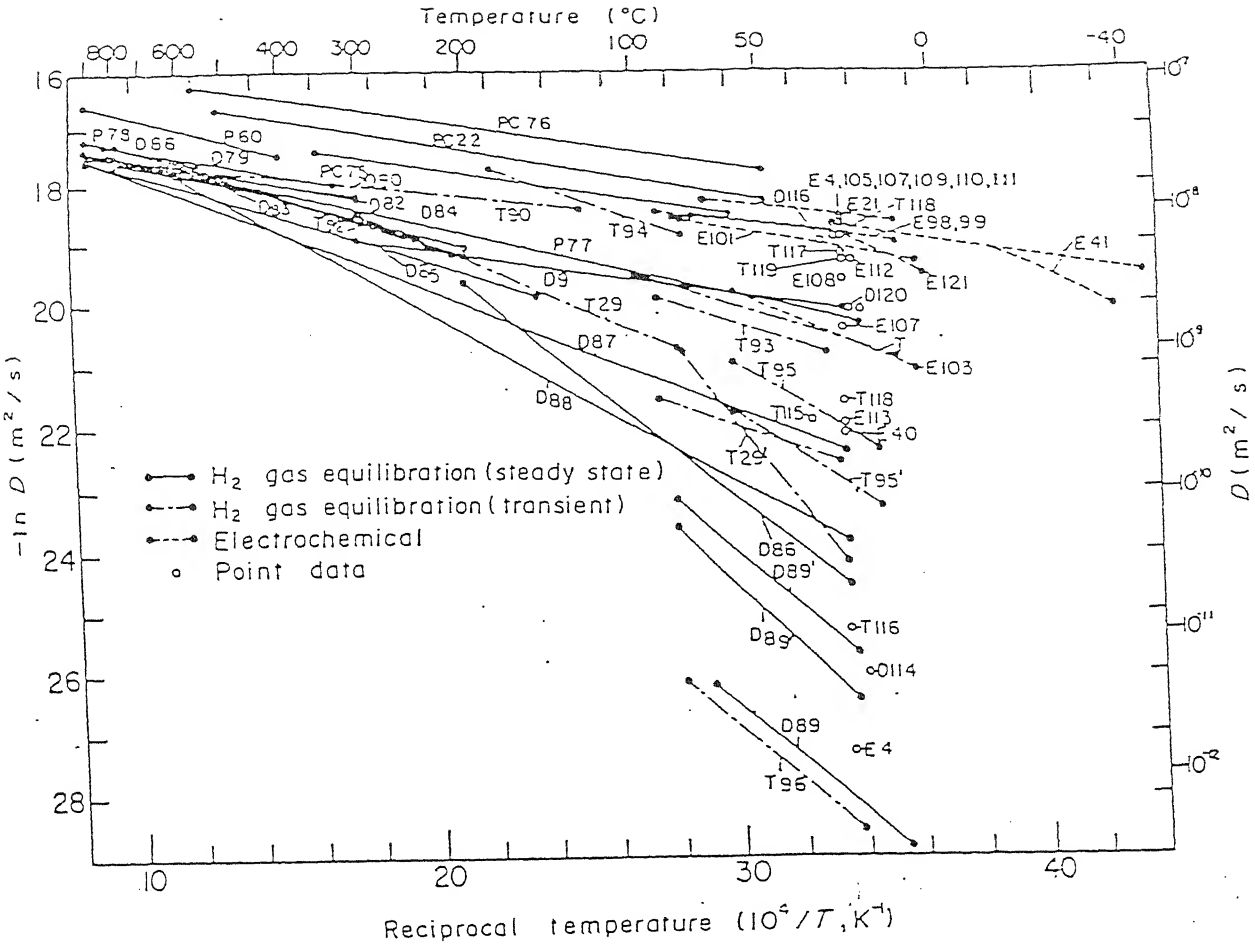

Figure 20. Arrehenius representation of diffusivity of hydrogen in α-Fe [38].

to be observed is the relatively large scatter in the experimental diffusivity data for hydrogen in iron, especially for temperatures lower than about 300K. This has been attributed to the errors in the experimental procedure which normally result in lower hydrogen diffusivity due to surface effects, defects in the surface regions like trapping sites, defects in the bulk region like dislocations and impurity atoms, and surface oxide effects [43]. From these figures, it can be seen that the room temperature diffusivity of H varies from 10^{-8} m^2/s to 10^{-12} m^2/s. Kiuchi and McLellan have carefully analyzed the diffusivity data for pure Fe and they conclude that the higher values are more reliable than the smaller ones [43]. Table 5 shows the diffusivity values of H in pure aluminum obtained by several researchers at 25^0C. In this table, all the data except that of Ishikawa and McLellan's have been obtained by extrapolation from higher temperatures.

There have been just two studies conducted on the diffusivity of hydrogen in Fe_3Al-based alloys. Chiu *et al* have employed an electrochemical permeation technique to measure the room temperature diffusivity of an alloyed Fe_3Al-based alloy, recently [64]. The alloy was ordered to get a B2 structure. The calculated diffusivity value was of the order of 10^{-9} m^2/s which they claimed was reasonable based on the fact that hydrogen diffusivity in b.c.c. metals at room temperatures were of the same order of magnitude. Hydrogen diffusivity in Fe-25Al was also determined using the subscale microhardness profiling technique by Banerjee after a recrystallization anneal of 4 h at 750^0C on a 1000^0C rolled sample and it was found to be 1.46×10^{-13} m^2/s. The effect of alloying (2%Cr, 2%Ti and 1%Cr-1%Ti) was also studied by Banerjee and it was noted that the diffusivity of hydrogen was an order of magnitude lower in these alloyed intermetallics compared to the base iron aluminide.

Table 5. Diffusivity of hydrogen in aluminium at 298 K obtained from the literature.

Investigators [ref]	Diffusivity D ($m^2 s^{-1}$)
W.Eichenauer *et al.*[a]	2.1×10^{-13}
W.Eichenauer *et al.*[b]	9.2×10^{-13}
M. Ichimura *et al.*[c]	1.5×10^{-12}
K. Papp *et al.*[d]	1.9×10^{-12}
T. Ishikawa *et al.*[e]	4.6×10^{-14}

a. W. EICHENAUER and A. PEBLER, *Z. Metallk.* 48 (1957) 373.

b. W. EICHENAUER, K. HATTENBACH and A. PEBLER, *Z. Metallk.* 52 (1961) 682.

c. M. ICHIMURA, M. IMABAYASHI AND M. HAYAKAWA, *J. Japan Inst. Metals* 44 (1980) 1053.

d. K. PAPP and E. KOVACS-CSETENY, *Scripta Metall.* 15 (1981) 161.

e. T. ISHIKAWA and R.B. McLELLAN, *Acta Metall* 34 (1986) 1091.

In the case of FeAl-based alloys, three diffusivity values have been reported. First, Zhu *et al* have provided a direct evidence of hydrogen generation from the reaction of water with Fe-38.5Al using laser desorption mass spectroscopy [4]. The hydrogen diffusivity has also been estimated from these profiles by Banners as 2.38 x 10^{-15} m^2/s [18]. Secondly, Kasual and Heldt [65] studied the kinetics of embrittlement of a B2 Fe-35Al polycrystal. The samples were cathodically charged with hydrogen. The rates of ductility recovery was measured by baking experiments, which indicated that the embrittlement was completely reversible. The rate of ductility recovery was utilized by Yang and Hanada [56] to estimate the room temperature diffusivity of hydrogen as 4 x 10^{-16} m^2/s.

Finally, Yang and Hanada [56] studied the hydrogen absorption and desorption in a ordered B2-40Al single and polycrystals (of mean diameter 500 μm). They studied the kinetics of hydrogen diffusion based on hydrogen content measurements after a heat treatment. Hydrogen was not charged but rather absorbed after exposures to the environment (relative humidity 60% at 20^0C) for different periods of time. They analyzed the kinetics of hydrogen diffusion from the hydrogen release data assuming that the material contained traps and that the lattice hydrogen concentration is higher than the trapped hydrogen concentration. From a plot of hydrogen concentration as a function of exposure time, the diffusivity of hydrogen was estimated by them to be 4.4 x 10^{-13} m^2/s. They used the value of the mean hydrogen content of the sample exposed in air for more than three months as the surface concentration. As they obtained a different diffusivity of hydrogen, they proposed that this could arise due to difference in the mechanism of absorption and desorption. It is also interesting to note that Yang and Hanada [56] found that hydrogen present on the surface desorbed at the lower

temperatures, whereas the hydrogen trapped in vacancies at a higher temperature and the hydrogen trapped at much higher temperatures was assigned by them to be due to trapping at grain boundaries. No conclusive evidences were provided by them for trapping at the grain boundaries. Finally, it must be pointed out that they did not electropolish the surface before exposure and therefore the possibility of surface trapping cannot be excluded. Therefore, the scatter in the data obtained for B2FeAl could also be due the above mentioned trapping effects.

2.7 HYDROGEN EMBRITTLEMENT MECHANISM

The process of HE is iron aluminides can be visualized as follows. The reaction that provides nascent hydrogen which embrittles iron aluminides is reaction (2) provided in section 2.2. The propensity of this reaction increases with increasing aluminum concentration in iron aluminides [5]. The reaction of condensed moisture from ambient environments with aluminum at crack tips and freshly created metal surfaces (due to oxide apallation) results in the generation of high fugacity atomic hydrogen that causes severe embrittlement. This process is schematically illustrated in Figure 21 [5].

Birnbaum *et al* have proposed a mechanism known as hydrogen enhanced localized plasticity (HELP) [66]. This mechanism suggests that hydrogen increases plasticity at the crack tip in many metals and alloys, leading to brittle fracture. There is a controversy about this mechanism that whether hydrogen influences plasticity through the volume or the surface. But there are enough evidences to prove slip localization due to hydrogen near a crack tip in several fcc and bcc metals [66]. However, in the case of iron aluminides, the fracture is essentially of cleavage type in

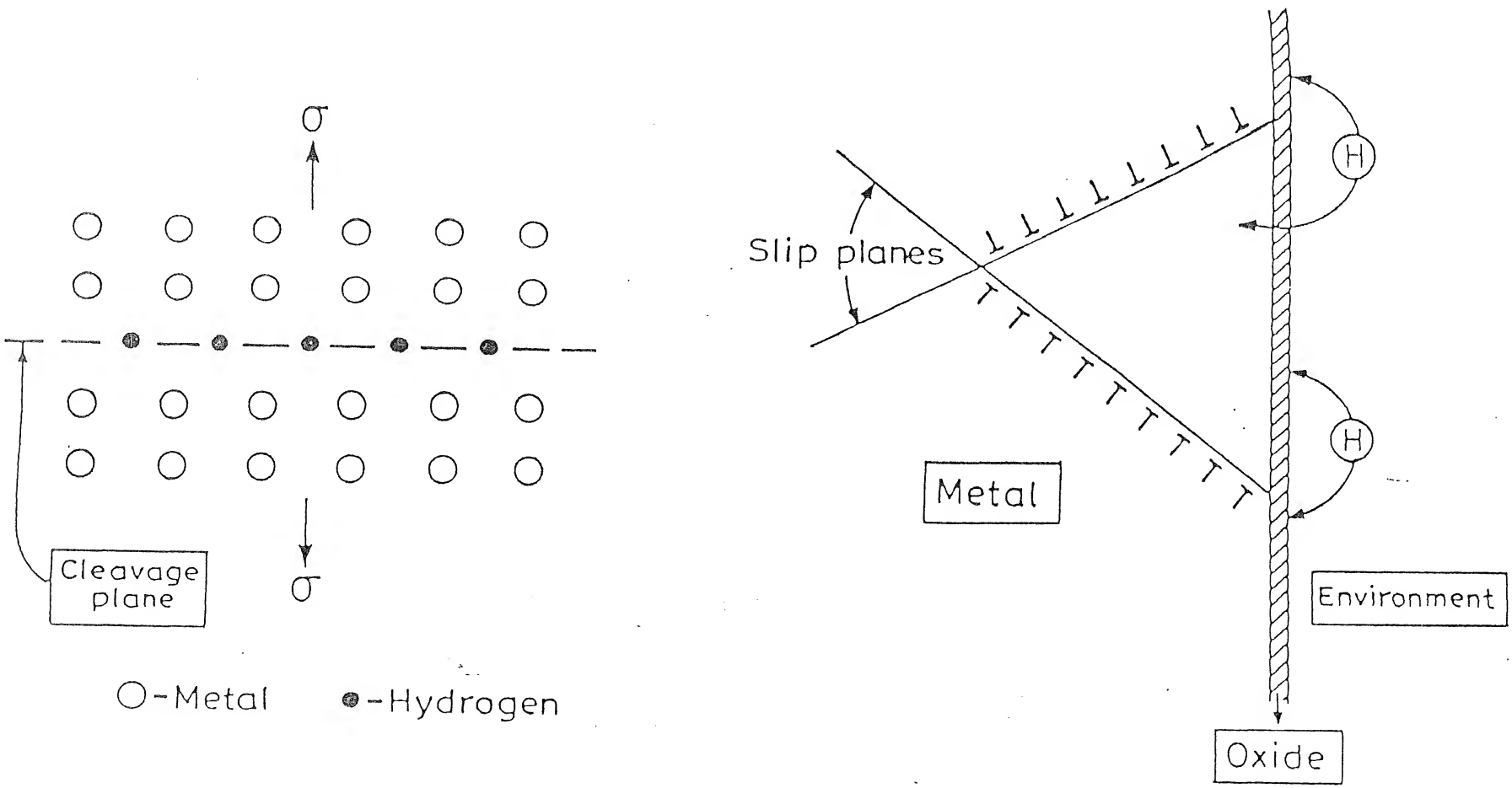

Figure 21. Hydrogen embrittlement mechnism by decohesion mechanism in iron aluminide [5].

the presence of hydrogen and therefore the HELP mechanism may not be applicable to the case of iron aluminides.

Generally, the fracture appearance in this class of intermetallics is of the cleavage type, with facets of {100} type suggesting "decohesion" as the possible mechanism of hydrogen embrittlement. The decohesion mechanism of hydrogen embrittlement is shown in Figure 22 [8]. Hydrogen enters the material after bulk diffusion or grain boundaries diffusion and absorption on the surface. This hydrogen is supposed to lower the bond strength in iron aluminides [8].

Evidence for decohesion mechanism is based upon the brittle appearance of fracture surface and the propensity for cleavage on {001} planes in embrittled single crystals of intermetallic aluminides [67]. Moreover, the brittle appearance of hydrogen induced (or moisture induced) fatigue cracks in iron aluminides alloys also suggests decohesion as the likely mechanism of hydrogen embrittlement [67]. In an earlier study, the presence of etch pits indicated the emerging points of some of these dislocations [10]. Most of these etch pits were of rectangular shape which indicated that the cleavage planes were of the {100} type. Therefore, the cleavage planes in Fe_3Al being of the {100} is not surprising as the structure of Fe_3Al is essentially BCC (i.e. disordered α at high temperature and ordered B2 and DO_3 at lower temperatures). The appearance of {100} cleavage facets suggests decohesion as the possible mechanism for hydrogen embrittlement (HE) in this class of intermetallics. Hydrogen enters the material and is transported to potential flaw sites by bulk or grain boundary diffusion or by dislocations sweeping in of hydrogen. The incoming dislocations are locked as immobile <100> dislocations [8]. Locked dislocation networks of this type have been observed by transmission electron microscopy within the grains [68] and

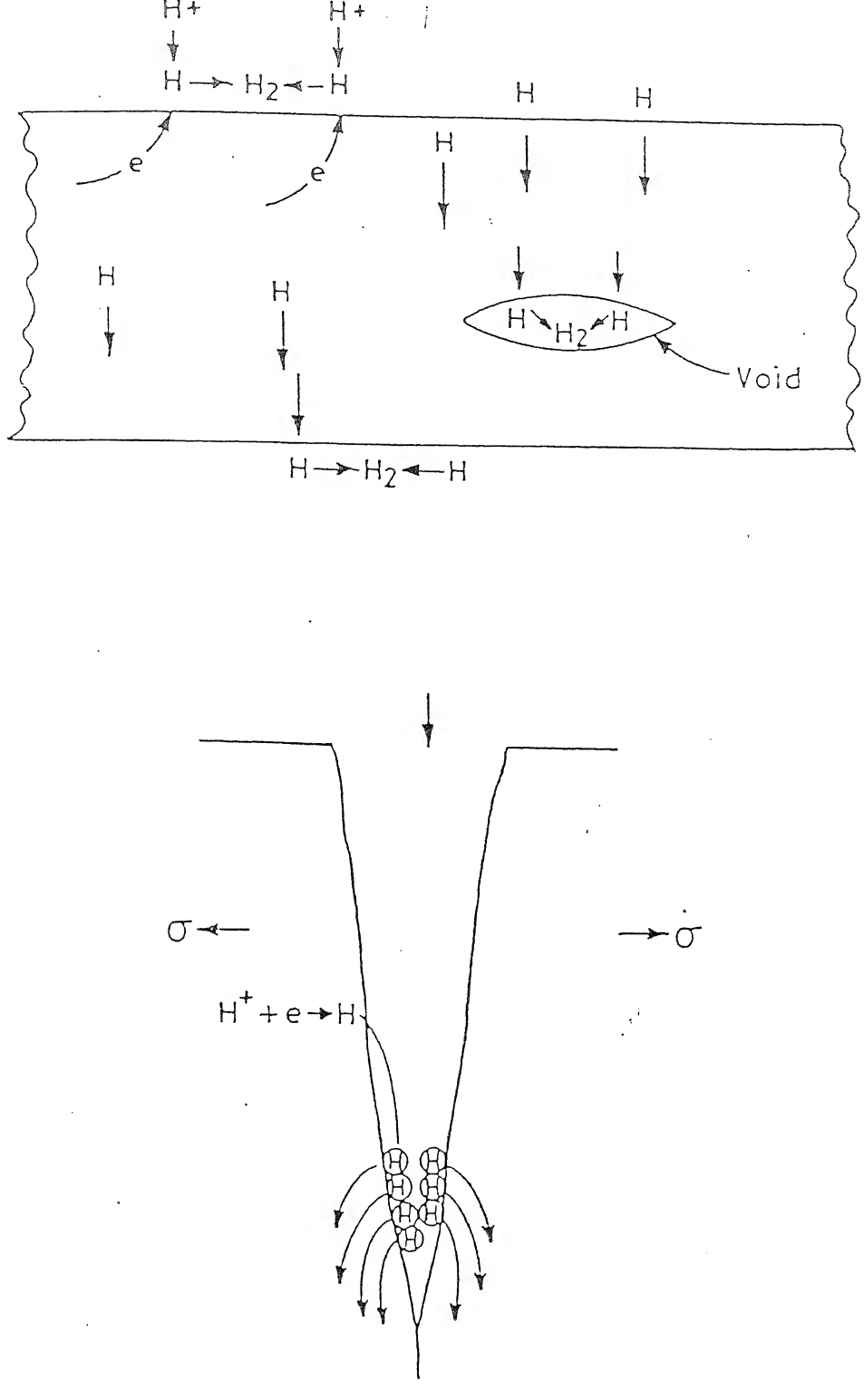

Figure 22. Hydrogen entry into the material and processes that occur at the crack tip during embrittlement [8].

grain boundaries [26] of deformed iron aluminides. Hydrogen promotes the formation of these locked <100> dislocations [35] and twice the amount of normal hydrogen can be trapped by these dislocations [35]. The amount of hydrogen should exceed a critical to cause cracking, as in well known in hydrogen embrittlement phenomenon. The critical limit to cause cracking should be a function of the stresses created in the hydrogen-occupied interstitial sites on the {100} planes of the ordered B2 and CO_3 [8]. the actual number of tetrahedral sites would depend upon the type of crystal structure (B2 or DO_3) but their presence in sufficient quantity aids hydrogen accumulation on the {100} plane leading to cracking by decohesion [8].

2.8 MAGNETIC BEHAVIOUR OF IRON ALUMINIDE

Alloys containing less than 33 at % aluminium are ferromagnetic in nature at room temperature. However certain of them in the region of Fe_3Al displays some remarkable anomalies in their magnetic behaviour [69].

Figure 23 [69] shows the effect of aluminium concentration on the magnetic saturation of iron. The magnetic saturation of iron falls slowly when aluminium is added almost as if reduced by simple dilution and only when 22% of aluminium is reached curve departs from linearity and sharp drop in saturation begins. It is observed that[69] this is a point when the lattice parameter is maximum. The magnetic saturation value falls to zero at 33% almunium i.e. Fe_2Al. This is precise point where the lattice parameter reaches its minimum and begins to rise again. It therefore proposed that the continued fall in lattice parameter between 22 to 33 at % aluminium is closely associated with the progressive loss of magnetic properties.

This stage occurs at Fe_2Al, approximately, where the magnetic saturation is virtually zero. At this point we entered a phase field in which, according to Hume

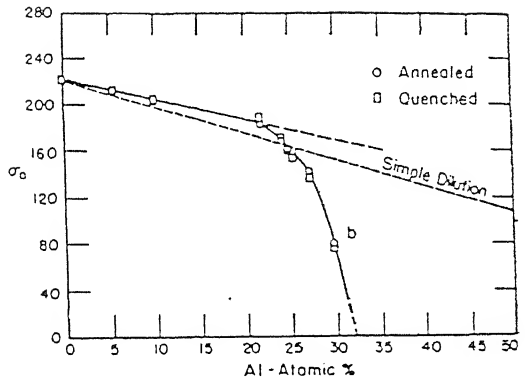

Figure 23. Magnetic saturation σ_0 of quenched and annealed alloy [69].

rothery rules the valency of the iron atom is effectively zero and the ratio of valency electrons to atom is 1:1 with continued addition of aluminium the ratio climb until it reaches its maximum 3:2 at FeAl. However if we assume that the magnetic moment of iron atom is due to the deficiency of 2.0 valency electrons in its d shell, there would not be enough valency electrons from the trivalent atom at the composition Fe_2Al to fill all the d-shell vacancies. There must consequently be some change in the energy levels of the d-shells or in the alignment of electron spins which effectively lead to a zero magnetic moment.

To resolve this point further we need neutron diffraction data over a whole series of iron-aluminium atoms and a data from soft x-ray absorption spectra which would give some insight into the nature of electron transfer.

It has been well established that cold working increases the lattice parameter and cause the destruction of long range order. Associated with the increase in lattice parameter and destruction of long range order is a considerable increase in saturation moment. Not only do the saturation moments of the alloys in the range $Fe_{13}Al_3$ to Fe_2Al increase, alloys which are normally non magnetic down to liquid helium temperatures become strongly ferromagnetic. Even FeAl shows traces of magnetism [69].

2.9 CURIE POINT

Considering the Figure 24 [69] according to interpretation of the data, there is definite break in the curie point curve where it meets the boundary bc separating the disordered α phase alloys from the α 2n alloys which have the FeAl type of order and which are non magnetic. The lower portion of the magnetic boundary coincides with the phase boundary. It may well be that this is not a curie point boundary in the normal

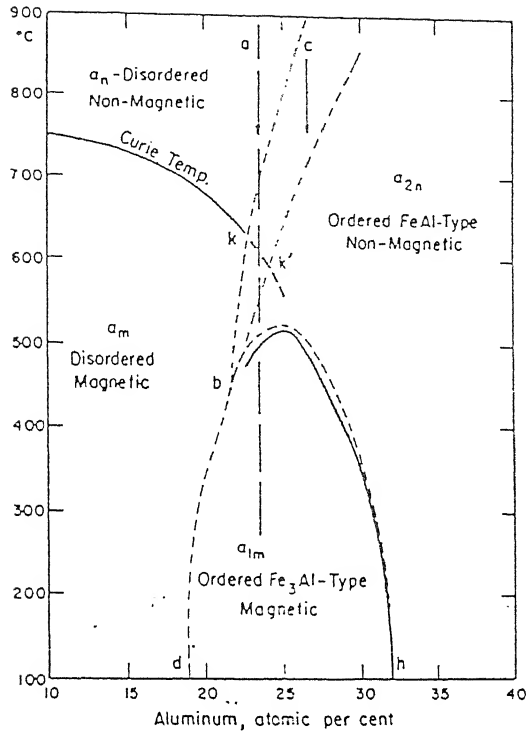

Figure 24. Lowering of transformation temperature with rapid cooling, permitting on set of ferromagnetism before FeAl type of ordering sets in [69].

sense, but is actually a boundary at which ferromagnetism is lost as a result of phase change.

By using a magnetic field of only 12 Oe so that their galvanometer deflection were proportional to the initial permeability in their specimens Sykes and Evans [70] found that alloys in the region of Fe_3Al exhibited two curie points on cooling. The induction at the upper curie point was greatest for the highest rate of cooling with the maximum displaced to some what lower temperature while the lower curie point was raised. A typical set of curves for different cooling rates for an alloy containing 13.4 weight per cent aluminium is shown in Figure 25 [70].

This some what anomalous display of two curie point is fully in accord with the equilibrium diagram shown in Figure 24 As an alloy with composition a is slowly cooled from the non magnetic disordered state α 2n FeAl type of structure, and on further cooling it orders to the Fe_3Al type and almost simultaneously becomes ferromagnetic on account of the close proximity of the magnetic and phase boundaries. Thus a slow rate of heating or cooling results in only one magnetic transformation namely the lower one. However if the same alloy is rapidly cooled the upper order disorder boundary bkc is depressed by an amount depending on the rate of cooling. The high temperature curie boundary for the disordered structure now extends beyond the composition k to k′ and the alloy becomes magnetic because it enters into now extended αm phase field. As temperature continues to fall, the delayed ordering transformation to the α 2n structure takes place and the alloy becomes nonmagnetic, only to become magnetic as the lower magnetic boundary is reached. The greater the rate of cooling the more the alloy finds itself in the αm magnetic phase field and greater the degree of initial magnetization. The depression of the boundary bkc thus

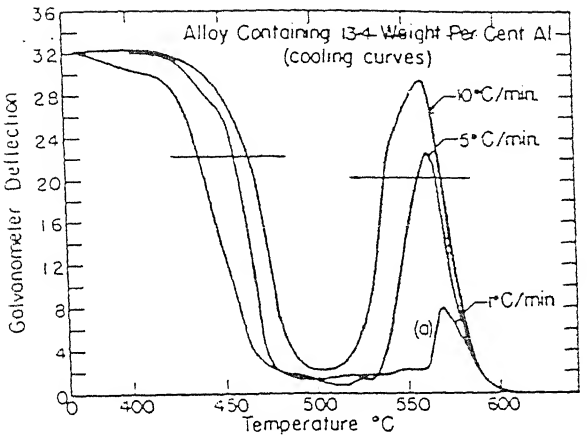

Figure 25. Double curie point phenomenon in iron aluminium alloys [70].

accounts for the greater initial magnetization setting in at lower temperatures. Similarly as indicated in Figure 25. The lower magnetic transformation is raised with increased rate of cooling, since the more disordered structure resulting from the greater cooling rate is more conducive to ferromagnetism.

CHAPTER 3

EXPERIMENTAL PROCEDURE

The chapter presents the details of materials used their associated processing and experimental techniques used for various characterization. The experimental methods mainly pertaining to hydrogen/deuterium charging followed by thermal desorption and magnetic evaluation have been presented.

3.1 MATERIALS:

The compositions of the iron aluminium intermetallics (pure and alloyed) were Fe-25Al, Fe-28Al, Fe-28Al2Cr, powder Fe-45Al, Fe-70Al. The Fe-25Al intermetallic was obtained from Defence Metallurgical Research Laboratory (DMRL), Hyderabad in the form of a pancake of diameter 120 mm and thickness 15 mm.

3.2 PROCESSING

The above pancake were further processed via ingot metallurgy route. In order to minimise segregation the pancakes were homogenized at 1000^0C for 4 hrs. Thin strips were sectioned from these using diamond wheel cutter. The virgin iron aluminide thin strips were rolled at 1000^0C (in disordered α-phase field). A total deformation of 80% was imparted to each of them in multipass rolling. All the strips had brown layer of oxide formed after rolling. Which were removed by abrasive polishing.

3.3 MAGNETIC MEASUREMENTS

The magnetic measurements were carried out with the help of a parallel field vibrating sample magnetometer (VSM) (Princeton Applied Research Model-150A) in conjunction with a Varian model V-7200 electromagnet assembly that provided magnetic field upto 11.5 KG (KOe). It measures the total magnetic moment of the

sample in electromagnetic units (emu). The temperature was controlled using an Indotherm, (model 401) temperature controller and an IC regulated power supply, (Network, model NPS 30/5D). A nickel chromium-nickel aluminum thermocouple aligned close to the sample inside the furnace indicated the temperature. The furnace chamber was evacuated using rotary and diffusion pumps during the heating process.

Samples of dimensions 3mm x 3mm x 2mm were sectioned and metallographically polished to 1 μm finish to remove any dirt or oxide present on the surface. These samples were weighed both before and after the magnetic measurements.

For study of powdered sample a novel method was tried. The cold setting powder used for mounting the sample was used for the preparation of pellet. A weighed mass of powder is transferred accurately to the die of 3mm internal diameter followed by mixing cold setting powder. The mixture of iron aluminide powder and the cold setting was set using cold setting liquid and allowed to set it for half hour. The problem here was the judicious selection of the mass of iron aluminide powder, cold setting powder and liquid so that the size of the pellet should not increase the above mention dimensions. Another problem was to transfer the weighed amount of iron aluminide powder in the die without weight loss. Hence a butter paper was selected instead of an ordinary paper so that the material should not stick to the paper while transferring the material into the die. These precautions were necessary to offset any inaccuracies in the calculation of the magnetic moment per gram.

3.4 HYDROGEN CHARGING STUDIES

The hydrogen and deuterium charging was carried out by three methods as discussed below.

CATHODIC CHARGING

For cathodic charging samples of approximately 10mm x 6mm x 2mm were sectioned for present study. The strips rolled at 1000^0C were used for this purpose. All the surface were polished metallographically to 1 μm finish followed by electropolishing (in electropolishing solution containing 15% perchloric acid and 85% methanol at a voltage of 15 volts for 5 minutes at temp of -30 C). The low temperature was maintained using liquid nitrogen. Samples were cleaned with acetone prior to cathodic charging in a specially designed electrochemical cell attached with a platinum counter electrode. The electrolyte used for hydrogen charging consisted of 0.1 N H_2SO_4 aqueous solution to which 100 ppm of sodium arsenate was added as a hydrogen recombination poison at room temperature (25 C).

The charging conditions were varied as below.

(i) charging current 10 - 20 mA/cm^2

(ii) electrolyte concentration 0.1 - 0.5 N H_2SO_4

(iii) charging time 12 to 60 hrs.

Deuterium was charged cathodically in D2O (Heavy Water) at a current density of 10 mA/cm^2 for 12 hrs.

3.5 DEPTH WISE CHARGING STUDY BY ERDA

ERDA can detect hydrogen upto a depth of 0.2 μm at the most. Hence to check what is happening below this level, the samples were thinned layer by layer using abrasive and electropolishing. The samples were weighed before and after polishing after monitoring different electropolishing parameters like solution strength,

electropolishing voltage and time. While polishing care was taken to mark the surface that was previously analysed under ERDA.

3.6 ERDA INSTRUMENTATIONS AND TECHNIQUES

The accelerator (High Voltage Engineering Corporation (HVEC) make, USA, (1968) is currently being utilized for material analysis using the nuclear techniques, viz. Rutherford backscattering, channeling, proton induced X-ray emission and elastic recoil detection of hydrogen and deuterium. It is equipped with a RF ion source and ion beams of hydrogen, helium, argon, krypton and other gaseous species can be obtained with a few microampere current on the target. The ion energy can be controlled to an accuracy of ± 1 KeV. Magnetically analyzed He^+ beam in the energy range of 1.4 to 1.8 MeV is used for ERD analysis. The beam is collimated using different apertures along its path to obtain divergence of $<0.05^0$. The collimated beam enters the ERD chamber through adjustable beam defining slits. The details of the chamber are shown in figure 26. It is mounted on a diffstack pumping system equipped with a liquid nitrogen trap to perform experiments in a clean and high vacuum of $<5 \times 10^{-6}$ mbar. The important components of the ERD set-up (i) holder for accurate positioning and orientation of the sample, (ii) secondary electron suppresser, (iii) arrangement to measure integrated charge, (iv) arrangement to mount and cool the silicon surface barrier detector and (v) mylar absorber to stop the forward scattered He^+ beam from reaching the ERD detector. The set-up also be utilized for RBS and channeling analysis using a detector mounted at an angle of 150^0 with respect to the beam direction. The ERD detector can accurately be positioned to make an angle varying from 20^0 to 40^0 with respect to the incident beam direction in a horizontal plane containing the incident beam. The aperture in front of the ERD

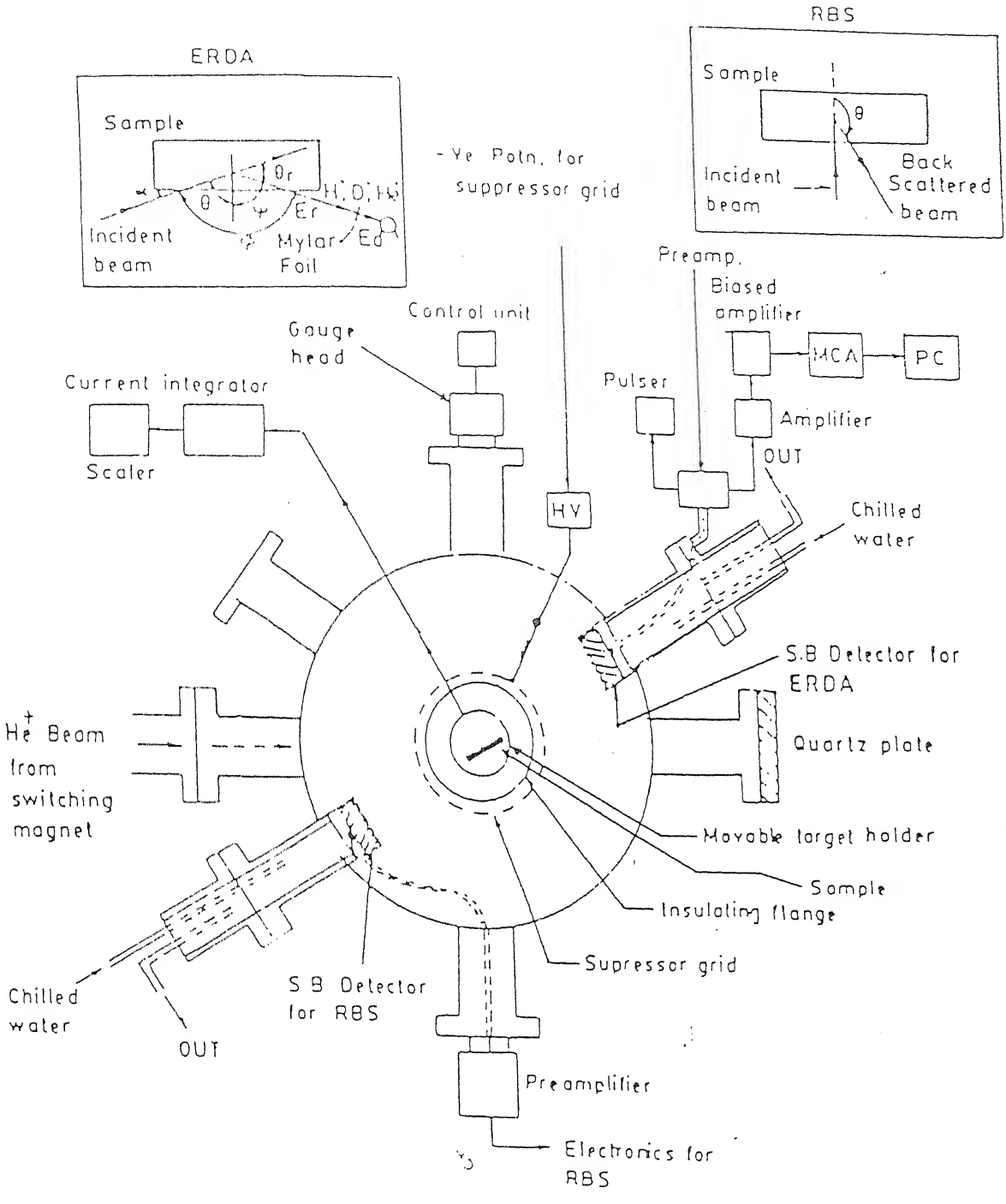

Figure 26. Block diagram of ERDA chamber and associated electronics.

detector has especially been designed to reduce the kinematical broadening. The signals from the detector are amplified using conventional nuclear electronics and are energy analyzed using a multichannel analyzer which is connected to a personal computer for data transfer.

2.5.1 ERD FORMULISM

The scattering geometry of ERD is shown in the left top inset of figure 26. The quantitative analysis of hydrogen and deuterium mainly involves three basic concepts: (i) kinematic factor (K), (ii) the differential recoil cross-section ($d\sigma/d\Omega$), and (iii) the stopping cross-sections of the incident and recoiled particles in the target.

The He^+ ion of incident energy E_o recoils H and D from the surface whose energy is given by

$$E_r = KE_o, \qquad (1)$$

where K is the kinematic factor given by

$$K = [4M_pM_r/(M_p + M_r)^2]\cos^2\theta_r, \qquad (2)$$

where M_p and M_r are masses of the projectile and recoiled atoms respectively. Also incident helium ions get scattered in the forward direction due to the heavier matrix elements. These scattered primary ions are stopped from reaching the detector by the stopper foil of appropriate thickness. Assuming surface energy approximation (Doyle and Peercy 1979), the energy of H or D getting recoiled from a depth x within the sample is given by

$$E_d = KE_o - [S]x - E', \qquad (3)$$

where [S] is the energy loss factor given by

$$[S] = \{K[dE/dx]^{He}/(\cos\theta)\} + \{[dE/dx]^r/(\cos(\theta + \theta_r)\} \qquad (4)$$

$[dE/dx]^{He}$ is the stopping power for He^+ at its incident energy and $[dE/dx]^r$ the stopping power for either H or D at the surface recoiled energy Ke_o and E′ the energy lost by the recoiled particles in the stopper foil. If the concentration (at./cc) of the recoiling species at a depth x in the sample be N(x) then

$$N(x) = Y/\{Q(d\sigma/d\Omega)\Omega(\delta E/R \sin \alpha[S])\} \quad (5)$$

where Y is the yield of recoils per channel at energy E_d, Q the total number of incident ions on the sample during the data acquisition time, δE the detected energy window per channel., R the ratio of the recoiled ion's stopping power in the absorber foil at energy E_r and E_d, $d\sigma/d\Omega$ the elastic recoil cross section, Ω the solid angle subtended by the detector and α the grazing angle which the incident beam makes with the sample surface as shown in the inset of figure 26. It should be noted that the recoil processes of hydrogen and deuterium from an incident He^- ion of energy ≥ 1 MeV are not purely Coulombic in nature. Therefore, the cross-sections given by Rutherford formula are not valid in this case. Because of the application potential of ERD of H and D using helium ions there has been a renewed interest for measuring the H (^{4}He, H) ^{4}He and D(^{4}He, D) ^{4}He cross-section data accurately (Besenbacher *et al* 1986; Wang and Zhou 1988; Baglin *et al* 1992; Quillet *et al* 1993). We have obtained linear fits to these data which have been used in the analysis. Several simulation codes namely RUMP (Doolittle 1985), SENRAS (Vizkelethy 1990), GISA3 (Saarilahti and Rauhala 1992) are now available for quick and accurate data analysis. We have installed RUMP simulation code for the analysis of the recoil spectra. The reader is advised to refer to, T. Som *et al* and V. N. Kulkarni, "ERD facility for analysis of hydrogen and deuterium in solids", Bulletin of Materials Science, Vol 19 No. 1 Feb. (1996), pp 73-82.

2.6 HIGH TEMPERATURE HYDROGEN CHARGING

The samples were placed in a quartz tube (4 cm internal dia and 3 ft in length) fitted with a pressure tight rubber quark. The tube had an opening for the gas inlet which is connected to the hydrogen gas cylinder and a outlet which is connected to the bubble indicator to indicate the gas flow. Hydrogen purging was done for 15 minutes at room temperature. Then the tube was inserted into the furnace kept at 800^0 C. Hydrogen pressure was kept above atmospheric pressure indicated by the digital meter. Hydrogen pressure was maintained after the heat treatment was over during cooling of the samples.

2.7 PLASMA HYDROGEN CHARGING

A sketch of plasma source for ion implantation is shown in Figure 27. The chamber is first evacuated to a base pressure of 10^{-6} torr using a turbomolecular pump. A flow of the gaseous species to be implanted is then established in the chamber to provide a final equilibrium pressure of 10^{-2}-10^{-3} torr. The plasma is generated by ionizing the gas and the sample is based to a negative potential of -3KV. As the sheath containing electrical field is formed, it shields the surrounding plasma from the applied potential. Ions within and at the edge of the sheath are accelerated by the electric field and travel through the sheath and are implanted into the sample. For the work described here, we have implanted -3KV hydrogen at the equilibrium pressure of 10^{-2} torr in electropolished iron aluminide for 1 hour.

2.8 HYDROGEN DESORPTION STUDY USING THERMAL ANNEALING

A schematic diagram of the annealing set up is shown in Figure 28. The furnace used for the annealing has a ceramic tube (i.d. = 2 inch), wound with nichrome wire with a uniform temperature (maximum 1000^0C) zone of 4 inch, length in the central portion of the ceramic tube. The furnace temperature is measured by a chromel

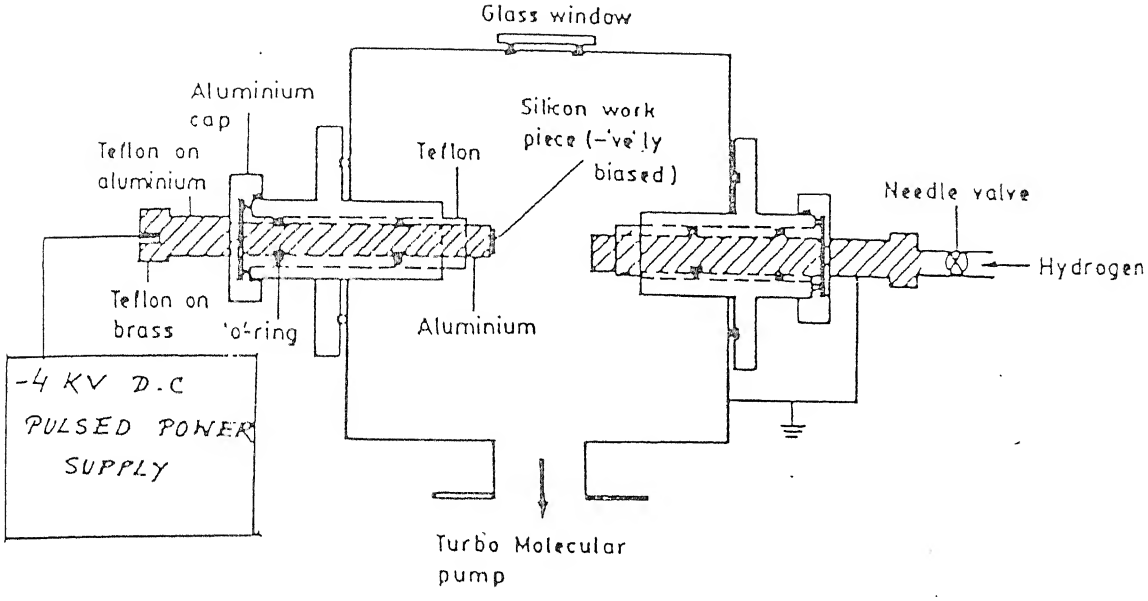

Figure 27. Schematic diagram of plasma source ion implantation set up.

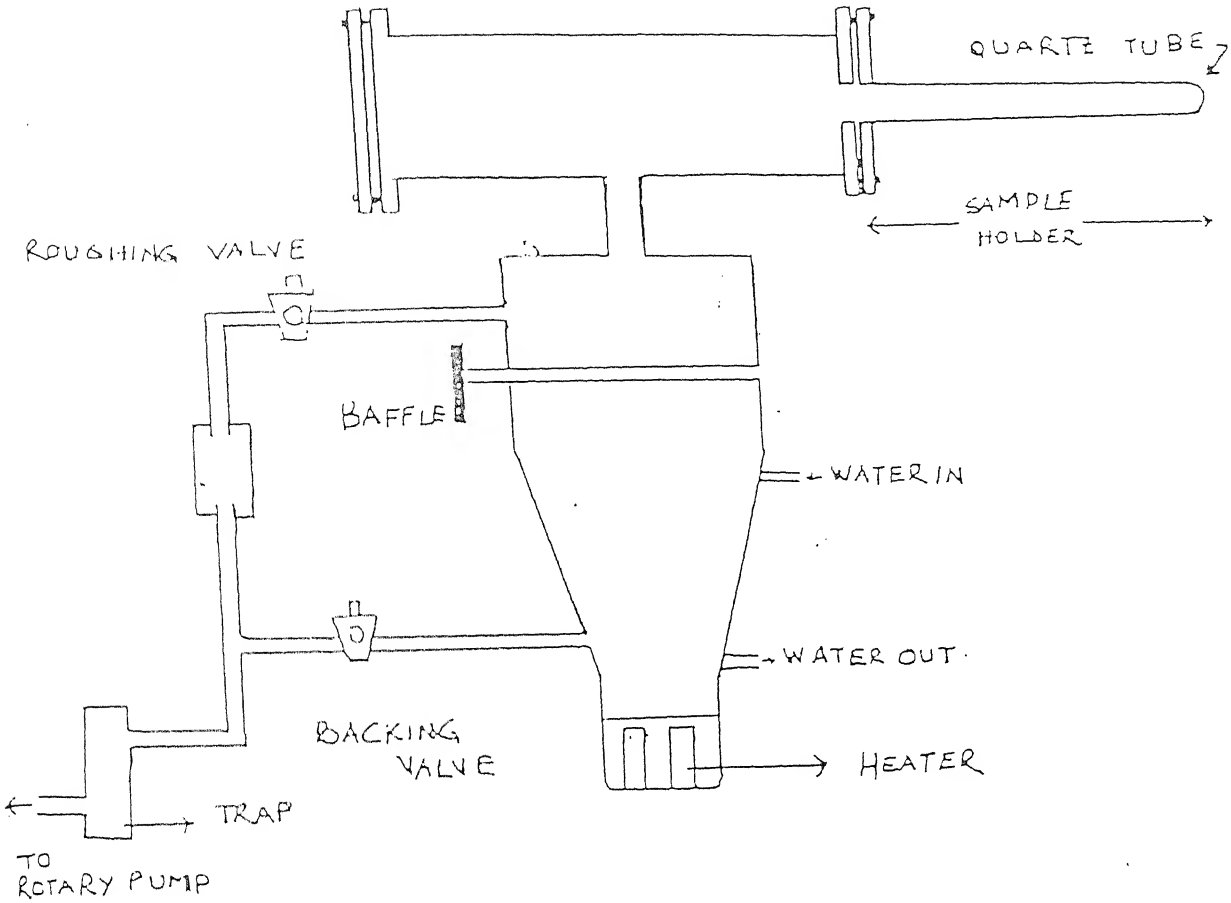

Figure 28. Schematic diagram of annealing chamber.

alumel thermocouple. The furnace temperature can be controlled to within ± 2^{0}C. The furnace is kept on a horizontal movable platform. The sample to be mounted are kept in the quartz tube (i.d. 1 inch) which is continuously evacuated by a diffusion pump equipped with a liquid nitrogen trap. After reaching the desired temperature, the furnace is moved such that the quartz tube containing the sample enters the central portion of the furnace. To achieve thermal equilibrium, on an average it takes two minutes during heating and five minutes during cooling. The thermal annealing was carried out at 450 - 500^{0}C for the duration of 15, 30 and 45 minutes under a vacuum of 5.5 x 10^{-5} torr. In the case of 450 C the hydrogen desorption was carried out for 15 minutes only.

2.9 ELECTROPOLISHING

Samples were electropolished to the same degree of smoothness to ensure the same absorption efficiency of iron aluminide for hydrogen contamination of the metal surface by oxygen or other foreign elements may retard the rate of chemisorption. Samples were also electropolished to remove the desired surface level of the hydrogen charged sample on which ERDA has been done and when it is felt that it is necessary to remove the top surface layer of required thickness without affecting chemistry of the sample.

Electropolishing data is given below: (Table 6)

15% perchloric acid in methanol solution temp -30 deg C

Voltage (V)	Current (A)	Time (Min)	Weight loss (mgm)	Sample Quality
12	0.25	10	41	excellent
7	0.25	5	8.6	excellent
4	0.15	2	3.4	good
4	0.12	1	2.15	average
5% perchloric acid solution				
10	0.5	7	10.5	excellent
7	0.5	5	11.13	excellent
4	0.25	4	6.26	good
4	0.12	2	2.26	poor

2.5% perchloric acid solution				
10	0.10	7	15.76	excellent
5	0.12	4	7.05	excellent
5	0.08	1	1.52	poor
1.25% perchloric acid solution				
5	0.08	5	6.43	excellent
5	0.08	2	4.3	average
5	0.08	1	2.92	poor
0.625% perchloric acid solution				
10	0.04	7	5.87	average
10	0.20	4	18.62	excellent
5	0.12	2	4.14	good
5	0.06	1	1.39	poor
0.12% perchloric acid solution				
5	0.01	2	0.34	poor
5	0.01	2	0.09	poor
8	0.01	2	0.32	poor
10	0.01	2	0.92	poor
10	0.01	4	0.82	poor

Above results clearly indicates that to get a good surface finish (mirror finish) by electropolishing one has to have a certain critical concentration of perchloric acid. In addition to that voltage applied must be above 8V and time of electropolishing must be atleast 5 minutes. It is a trade off between concentration voltage and time to get excellent quality surface finish.

However it was not possible to exactly remove weight corresponding to 1 μm surface removal, when it was achieved the sample quality gone bad. At the most it is possible to remove weight corresponding to 5 μm accurately with excellent surface finish.

CHAPTER 4

RESULTS AND DISCUSSIONS

4.1 ELECTROLYTIC HYDROGEN CHARGING:

It has been well established that the poor ductility of iron aluminides at ambient temperature is due to hydrogen embrittlement. Hydrogen is produced by the reaction of moisture with the iron aluminide [4] and enters the lattice to cause embrittlement. Therefore one of the important factor that needs to be understood is the absorption of hydrogen in iron aluminides lattice.

Mao and Qiao have shown experimentally [71] that cathodic charging at current density of 10 mA/cm^2 and charging voltage of 3V for 20 minutes of Fe-25Al with hydrogen makes it more prone to embrittlement incomparision to virgin Fe-25Al. Cracking rate was higher than that without charging and the radius of crack tip was smaller than 1 nm as compared to crack tip radius of 3-70 nm in the uncharged specimens.

In a recent paper Zhu *et al* have provided [4] direct evidence for the production of hydrogen by reaction of moisture with iron aluminide (Fe-36Al). They have also used a laser desorption mass spectroscopic technique [4] to detect the presence of hydrogen in cathodic charged samples, water treated sample and virgin sample with removal of material using pulsed laser they were also able to obtain three dimensional distribution of internal hydrogen atoms as a function of depth from the surface after the iron aluminide was cathodically charged in 1N H_2SO_4 for one day. As shown in Figure 29 [4] they reported the strength of hydrogen signal in milivolt as a function of concentration depth qualitatively.

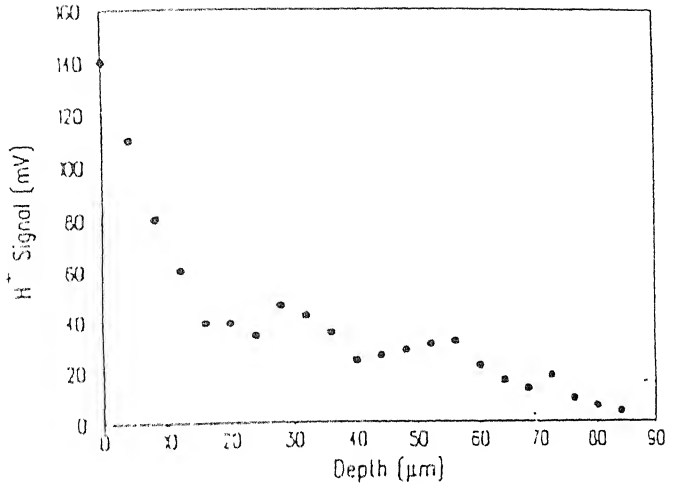

Figure 29. Hydrogen depth distribution measurements. The laser repetition rate is 10 Hz with laser fluence at 380 mJ/cm^2 [4].

However, they were unable to give quantitatively concentration. Similarly other workers have related hydrogen content of there intermetallics with microhardness and ductility [12, 18]. This group of workers again have not been able to give quantitative evaluation of hydrogen in the intermetallic.

The present work therefore is an attempt to obtain quantitative evaluation of lattice hydrogen of Fe-Al intermetallic.

Figure 30 shows the hydrogen recoil energy spectra from the samples which were cathodically charged with H_2 in 0.1 N H_2SO_4 at a current density of 10 mA/cm^2 for 12 hrs. The spectra clearly shows that there is profuse quantity of hydrogen in the sample. The maximum amount of hydrogen was obtained to be 33% on the surface and it drops to 7% at 1500 ^{0}A depth in a linear fashion as obtained by simulation. In order to obtain the maximum depth of hydrogen diffusion in the samples surface on which the measurements were taken removed systematically by metallographic polishing to 6 μm. At this depth only negligible amount of hydrogen was detected.

In the present electrolytic charging condition, it can be concluded that 6 μm is the limit. However this result is in strong contradiction with that of Zhu *et al* [4] who have been able to diffuse hydrogen up to the depth of 90 μm. There experimental conditions except the charging current density were different. They used solution concentration 10 times higher than ours and the charging times two times layers.

Hence another experiment was carried out in which we increased the solution strength from 0.1 N H_2SO_4 to 0.5 N H_2SO_4, (five times), the charging time was increased to 24 hrs (two times) and the current density from 10 mA/cm^2 to 20 mA/cm^2 (2 times). Figure 31 shows the hydrogen recoil energy spectra. Interestingly the maximum hydrogen concentration in this case was found to be only 4.2% as compared to 33% in the specimen charged with low concentration, low current density and less

However, they were unable to give quantitatively concentration. Similarly other workers have related hydrogen content of there intermetallics with microhardness and ductility [12, 18]. This group of workers again have not been able to give quantitative evaluation of hydrogen in the intermetallic.

The present work therefore is an attempt to obtain quantitative evaluation of lattice hydrogen of Fe-Al intermetallic.

Figure 30 shows the hydrogen recoil energy spectra from the samples which were cathodically charged with H_2 in 0.1 N H_2SO_4 at a current density of 10 mA/cm^2 for 12 hrs. The spectra clearly shows that there is profuse quantity of hydrogen in the sample. The maximum amount of hydrogen was obtained to be 33% on the surface and it drops to 7% at 1500 ^{0}A depth in a linear fashion as obtained by simulation. In order to obtain the maximum depth of hydrogen diffusion in the samples surface on which the measurements were taken removed systematically by metallographic polishing to 6 μm. At this depth only negligible amount of hydrogen was detected.

In the present electrolytic charging condition, it can be concluded that 6 μm is the limit. However this result is in strong contradiction with that of Zhu *et al* [4] who have been able to diffuse hydrogen up to the depth of 90 μm. There experimental conditions except the charging current density were different. They used solution concentration 10 times higher than ours and the charging times two times layers.

Hence another experiment was carried out in which we increased the solution strength from 0.1 N H_2SO_4 to 0.5 N H_2SO_4, (five times), the charging time was increased to 24 hrs (two times) and the current density from 10 mA/cm^2 to 20 mA/cm^2 (2 times). Figure 31 shows the hydrogen recoil energy spectra. Interestingly the maximum hydrogen concentration in this case was found to be only 4.2% as compared to 33% in the specimen charged with low concentration, low current density and less

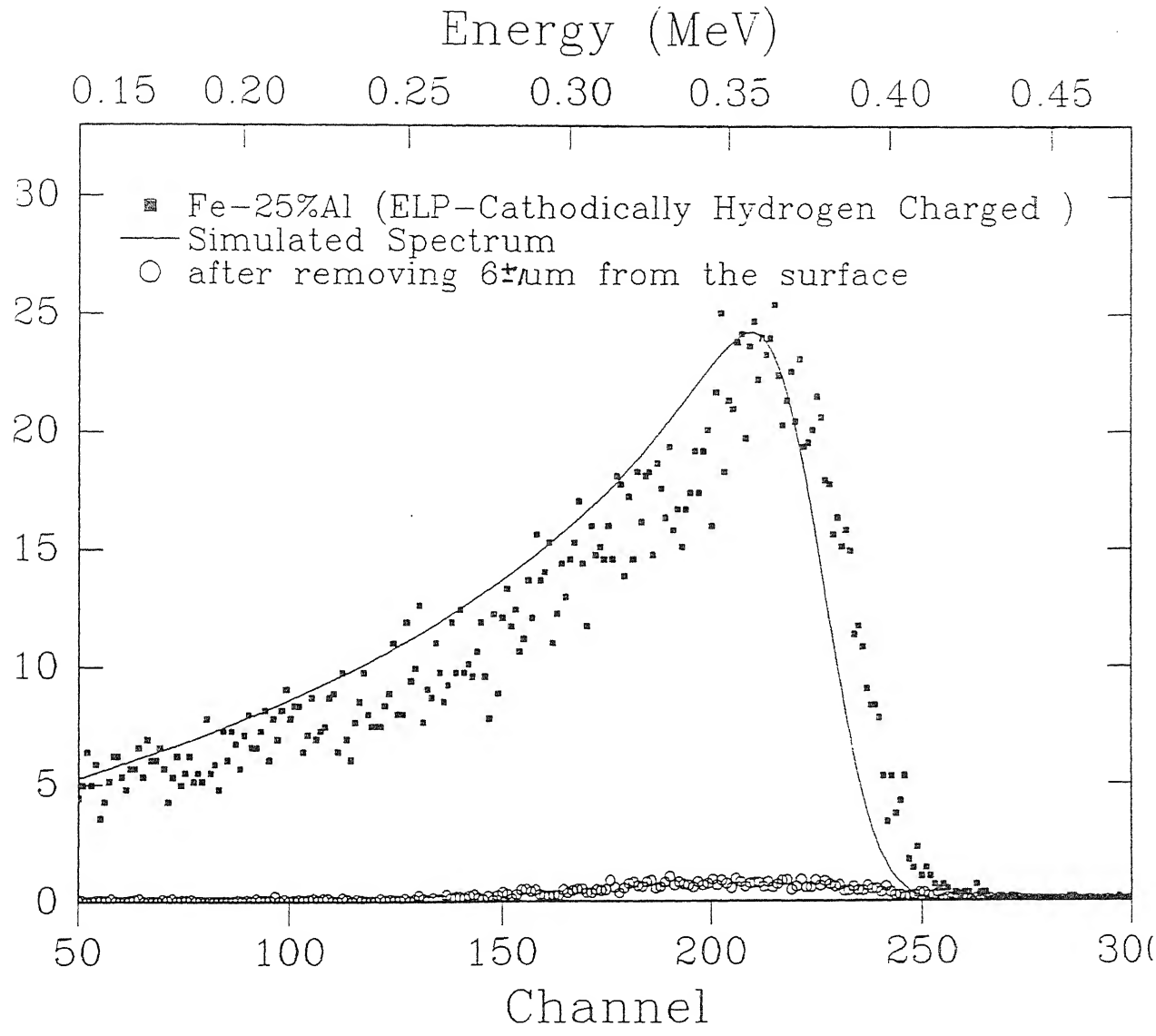

Figure 30. Hydrogen recoil energy spectra from the samples cathodically charged with H_2 in 0.1 N H_2SO_4 at a current density of 10mA/cm^2 for 12 hrs

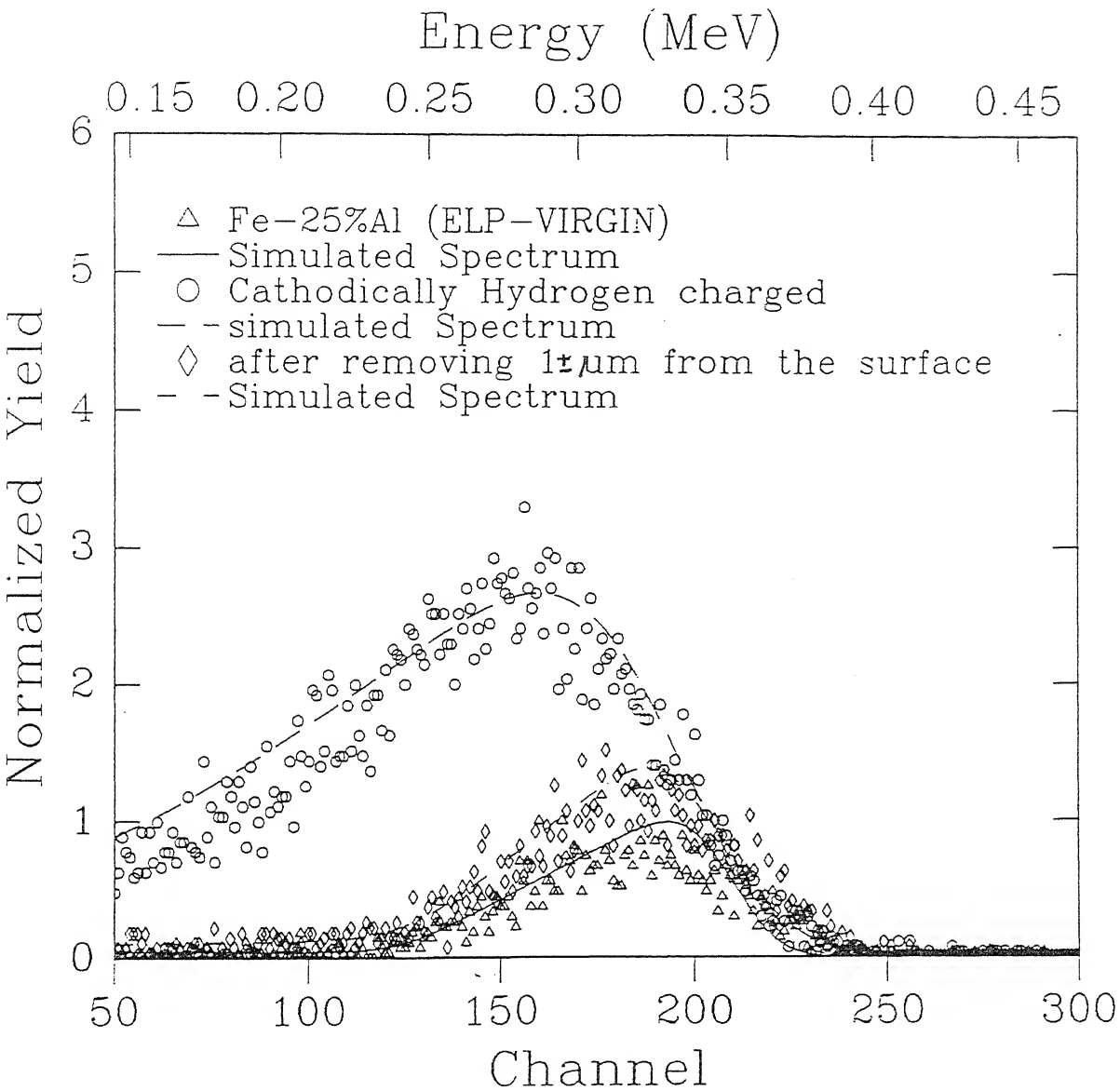

Figure 31. Hydrogen recoil energy spectra from the samples cathodically charged with H_2 in 0.5 N H_2SO_4 at a current density of 20mA/cm^2 for 24 hrs.

time at temperature of 20^0C. Also the maximum depth of diffusion was found to be 1 μm only. The results were surprising. The reason for this anomaly may possibly be due to higher temperature. As this experiment was carried out in the summer (night) the temperature must be in the range of 25-30^0C.

However, the maximum depth of hydrogen diffusion given by Zhu *et al* is 90 μm. But he has not mentioned the hydrogen concentration at this depth. A careful observation of his results (Figure 29) indicates that in his experiments the hydrogen concentration which he has given in terms of milivolt drops drastically (140 mV to 40 mV) from the surface to 10 μm depth. Beyond this it drops again at a very very slow rate. However he has not mentioned that about how many volts corresponds to what hydrogen concentration. It might turn out that the hydrogen concentration detected after 10 μm is very very low most probably in ppm which is beyond the range of detection of our instrument (0.1 atomic %).

Hydrogen diffusion coefficient obtained from the above experiments by using equation $x = \sqrt{Dt}$ is given and compared with the literature in the following table.

Table 7 diffusivity of hydrogen in the iron aluminide at 298 K obtained from the literature.

Material	Diffusion Coefficient (m^2/s)	Reference
Fe-25Al	1.46×10^{-13}	Banergee et al [18]
Fe-25Al	1×10^{-9}	Chiu et al [64]
Fe-25Al	8.33×10^{-16}-1.15×10^{-17}	Present study
Fe-38.5Al	2.38×10^{-15}	Zhu et al [4]
Fe-40Al	4.4×10^{-13}	Yang et al [56]
Fe-40Al	4×10^{-16}	Kasual et al [65]

4.2 HIGH TEMPERATURE HYDROGEN CHARGING BY PRESSURIZATION:

Figure 32 shows the hydrogen recoil energy spectra obtained from Fe-25Al charged by direct pressurization of H_2 gas at 800^0C for 3 hrs. It shows the comparison between the metallographically as polished virgin sample and that charged with hydrogen.

It is evident from the spectra Virgin sample also contains small amount of hydrogen. Hydrogen charging increases the concentration to 2.85%. this concentration is however much less incomparison to room temperature electrolytically charged samples. Similar effect has been observed [72] other workers on Fe.

This implies that the molecular hydrogen is less effective in diffusing into the aluminide. Only atomic and ionic hydrogen has tendency to diffuse easily into the material. Presence of hydrogen in the virgin sample gives the evidence that the hydrogen has diffused due to splitting of water molecule on intermetallic. As water is used in polishing, this high fugacity hydrogen generated must have diffused into the material during polishing process.

4.3 HYDROGEN INCORPORATION BY PLASMA ION IRRADIATION

Figure 33 shows the hydrogen recoil energy spectra after the plasma ion irradiation of electropolished sample for 1 hrs. The maximum hydrogen concentration was found to be 11.75% which is much more than the virgin sample and greater than the hydrogen charged by pressurization at 800^0C for 3 hrs (2.85%). In the plasma, atomic/ionic hydrogen is produced. This diffuse under electrical field directly into the material.

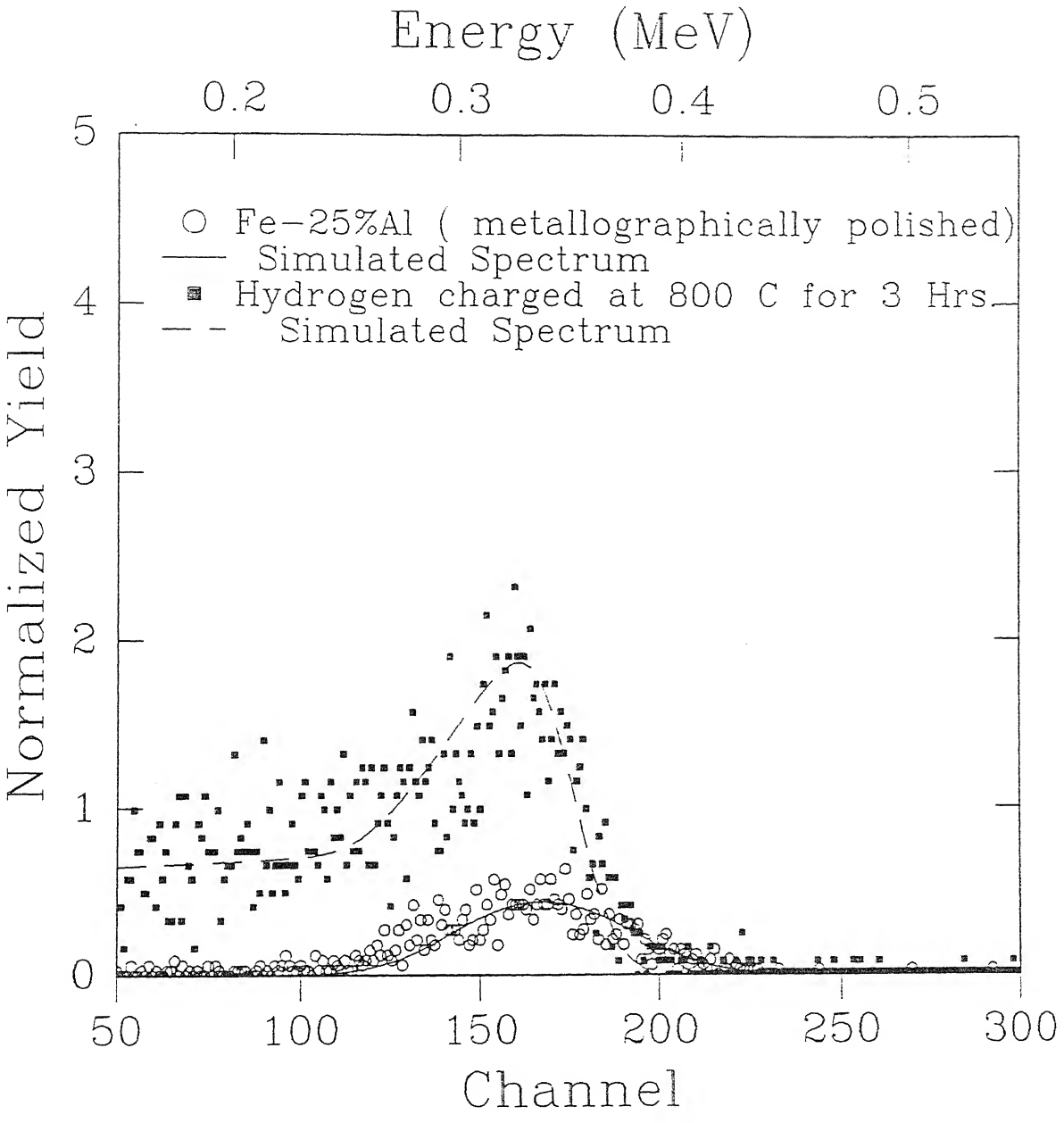

Figure 32. Hydrogen recoil energy spectra obtain from Fe-25Al charged by direct pressurization of H_2 gas at 800^0 C for 3 hrs.

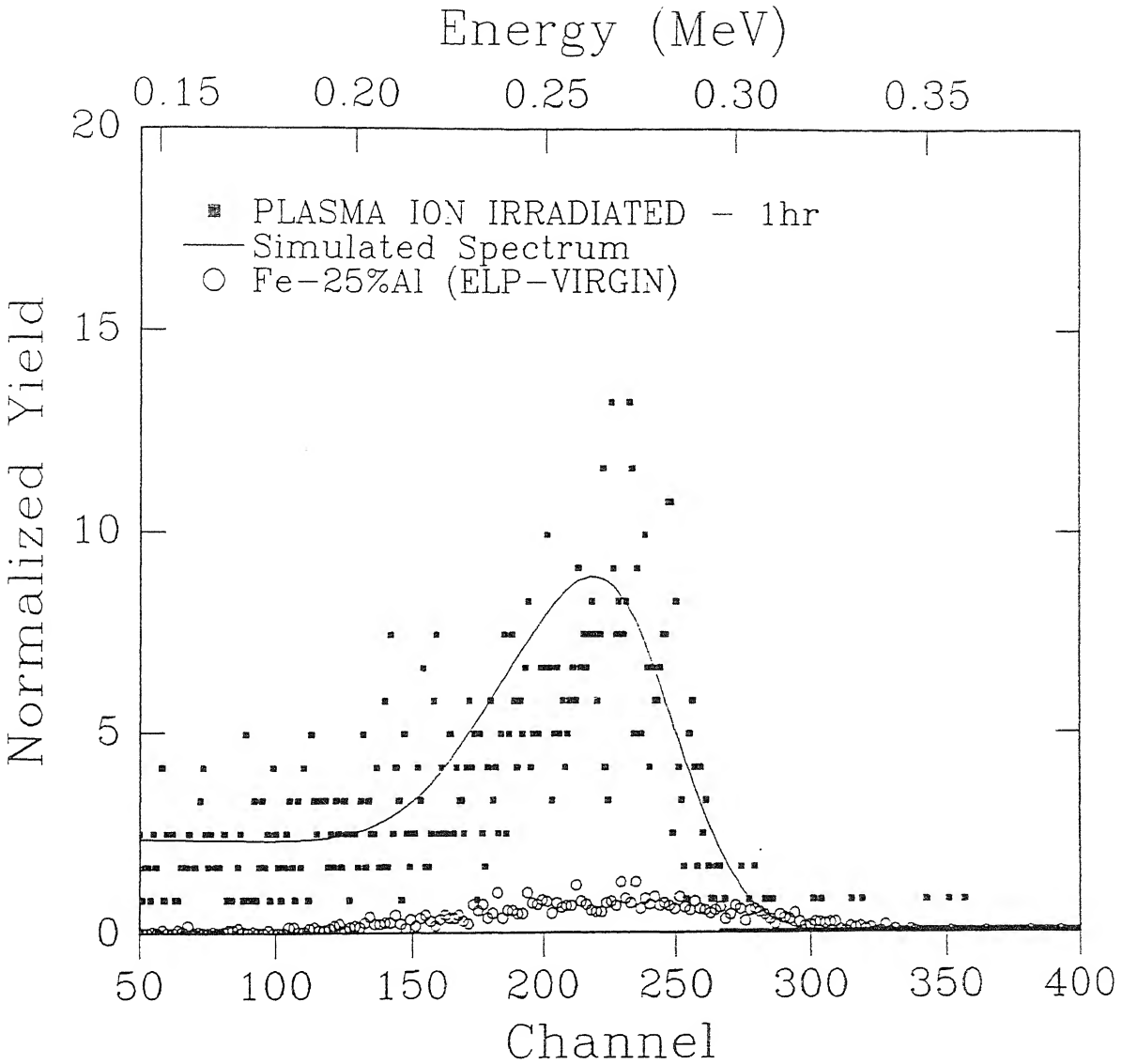

Figure 33. Hydrogen recoil energy spectra obtained.from Fe-25Al after the plasma ion irradiation of electropolished sample for 1 hrs.

4.4 HYDROGEN DESORPTION FROM HYDROGENATED Fe-25Al INTERMETALLIC

For this experiment samples were cathodically charged with H_2 and D_2 using D_2O electrolyte at 10 mA/cm^2 for 12 hours. The ERDA indicated (Figure 34) preponderance of H_2 incomparison to D_2 in the samples. The presence of hydrogen is attributed to the phenomenon called "PHOTO-DECOMPOSITION" of heavy water into the water. This is not surprising as the heavy water used in this experiment is more than 10 years old. This however offered unique opportunity to study both the H_2 and D_2 absorption/desorption process in the intermetallic.

Figure 34 shows the hydrogen and deuterium recoil spectra as of the cathodically charged samples. As evidenced from the spectra, deuterium is found on the higher energy side beyond 0.4 MeV than the hydrogen below 0.4 MeV. The recoil energy, using 1.25 MeV 4 He^+ irradiation and recoil angle of 30^0 was calculated to be 0.6 MeV and 0.83 MeV for H_2 and D_2 respectively. Since deuterium nuclei recoiling from the surface receives a higher fraction of (2/3) incident energy (E_0) than do hydrogen nuclei (1/3), the peaks in the spectrum are well separated in energy. A mylar foil is placed in front of the detector to block out He^- ions, scattered from the material. The mylar absorber introduces energy straggling leading to shift in energy. Two distinctive peaks numbered as peak 1 and peak 2 below 250 channel number are clearly visible for hydrogen in the D_2O charged sample. The first peak (normalized yield height of 7.5) corresponds to sample surface and second (normalized yield height of 10) corresponds to a depth of 700 ^0A. This shows a slightly higher concentration of H_2 just below the surface.

The second third and fourth curves from the top in Figure 34 are after vacuum annealing of sample at 450^0C for 9000 seconds, 500^0C for 9000 seconds and 500^0C for

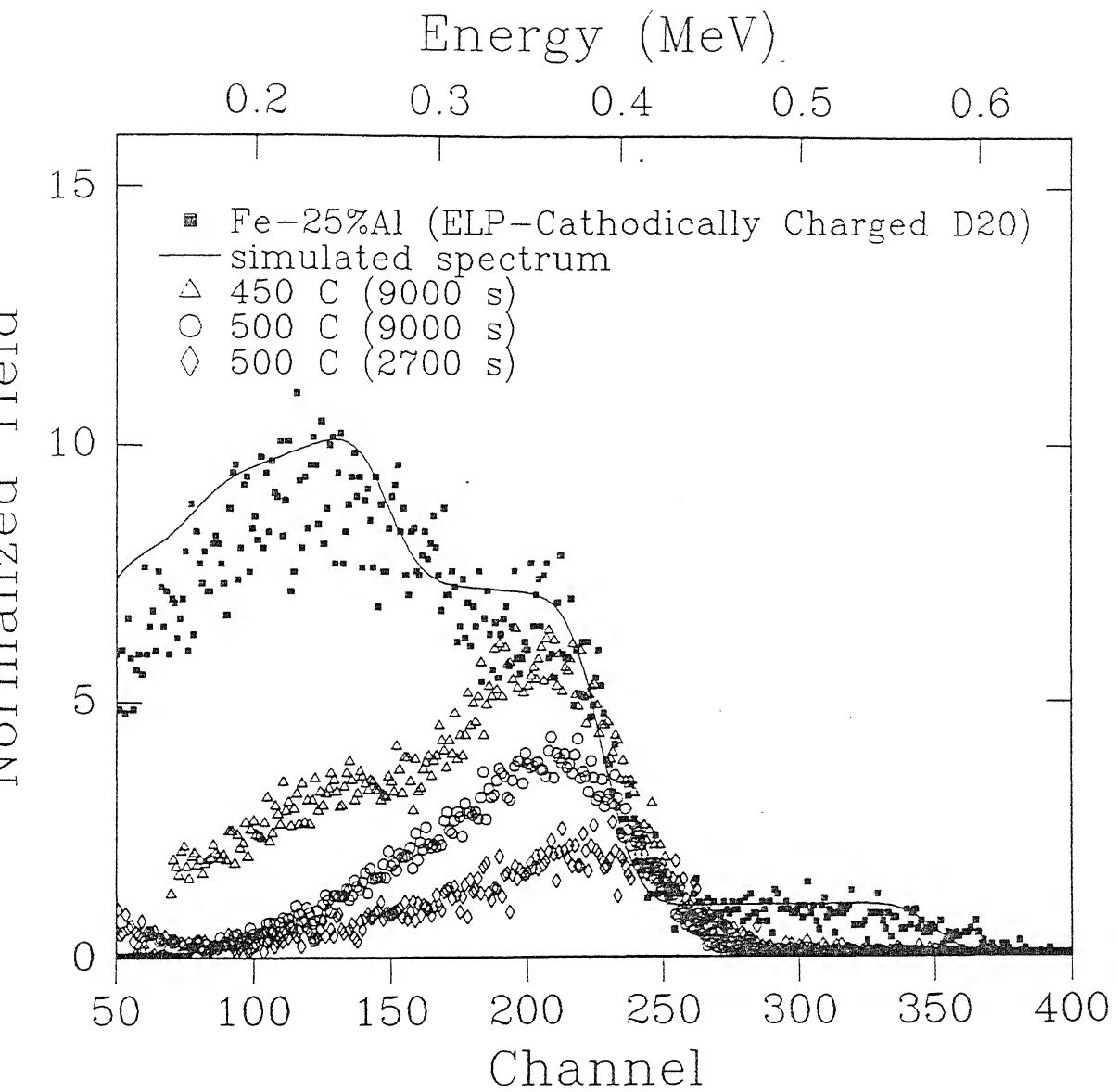

Figure 34. Hydrogen and deuterium recoil spectra obtained from Fe-25Al cathodically charged in D_2O (Heavy water) at a current density of 10mA/cm^2 for 12 hrs.

27000 seconds respectively. Thus during desorption, the surface has tendency to maintain higher amount of H_2 incomparison to interior of the samples. i.e. the intermetallic surfaces probably tries to maintain a higher amount of H_2 concentration than the interior. The hydrogen desorption rate initially was higher.

Deuterium is completely removed at 450^0C and there is only traces of deuterium after this treatment. This implies that the deuterium desorption temperature is lower than the hydrogen desorption.

4.5 MAGNETIC MEASUREMENT

In the pure iron, ferromagnetism occurs due to parallel spin alignment of unbalanced electrons in the 3d band. It is also known that the 3d band and the $4s^2$ valence band overlaps and atomic magnetic moment comes down to 2.22 μB per atom from about 4 μB for isolated Fe atoms. Alloying Fe with Al introduces extra electrons at the valence band and therefore depending upon possibility of electrons transfer from Al to Fe, the atomic magnetic moment of Fe will change. This will happen also with introduction of H_2 atoms into the Fe-Al intermetallic lattices as $4s^1$ electrons are highly mobile. Thus from changes in saturation magnetization, one could easily calculate electron transfer i.e. introduction of hydrogen atoms in the Fe-Al intermetallic. Visualizing this possibility, the study of effect of alloying on saturation magnetic moment has therefore been undertaken in the present work.

4.5.1 MAGNETIC BEHAVIOUR OF Fe-Al INTERMETALLIC AND ALLOYING EFFECT

Figure 35 shows the magnetic saturation obtained from two different samples of Fe-25Al. Near about 16% difference in the saturation values were obtained. It indicates deviation in composition due to segregation in the material which ultimately affected the magnetic saturation Figure 36, Figure 37 and Table 8 shows the effect of aluminium concentration on the magnetic saturation of iron. It falls continuously with aluminium addition. This reduction in Ms correspondence to dilution by Al atoms. Beyond 22% Al addition in Fe leads to departure from linearity and sharp drop in Ms begins as shown in Figure 37 It is observed that [69] this is the point when the lattice parameter is maximum. The magnetic saturation value falls to zero at 33% aluminium i.e. Fe_2Al. This is precise point where the lattice parameter reaches its minimum and begins to rise again. It therefore proposed that the continued fall in lattice parameter between 22 to 33 at % aluminium is closely associated with the progressive loss of magnetic properties due to weakening in ferromagnetic exchange interaction. Alternatively it has been proposed that in the α 1m ferromagnetic phase field there are two types of iron atom in Fe_3Al namely (i) those surrounded by 4Al atoms and 4 Fe atoms nearest neighbour and.(ii) those surrounded by 8 Fe atoms at the corners of the elemental cube. If the tetrahydrelly surrounded iron atoms were to absorb electrons from the surrounding atoms into their d-shells, their magnetic moment should fall and so should the ionic radii of aluminium atoms. This would lead to a progressive fall of magnetic saturation moments and lattice parameter, as more valence electrons are absorbed by 3d band with continued aluminium addition. Alternatively 4s electrons from the outer orbits of the iron might enter the 3d-shells with similar results, except that it would now be the atomic radii of the iron atoms which would be decreased.

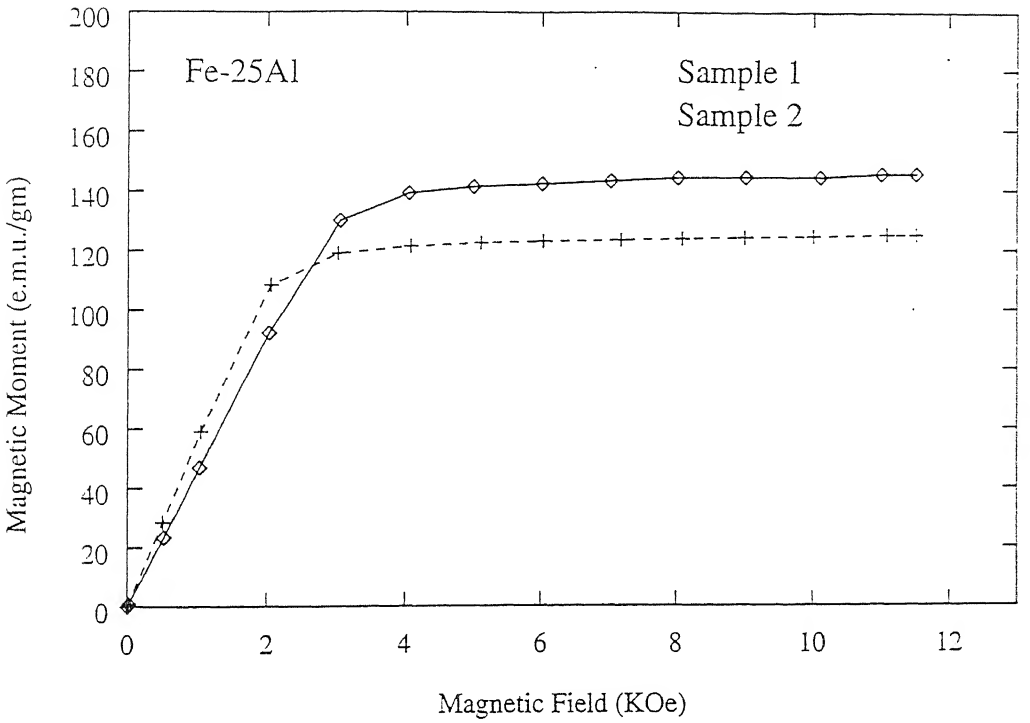

Figure 35. Magnetic saturation obtained from two different samples of Fe-25Al.

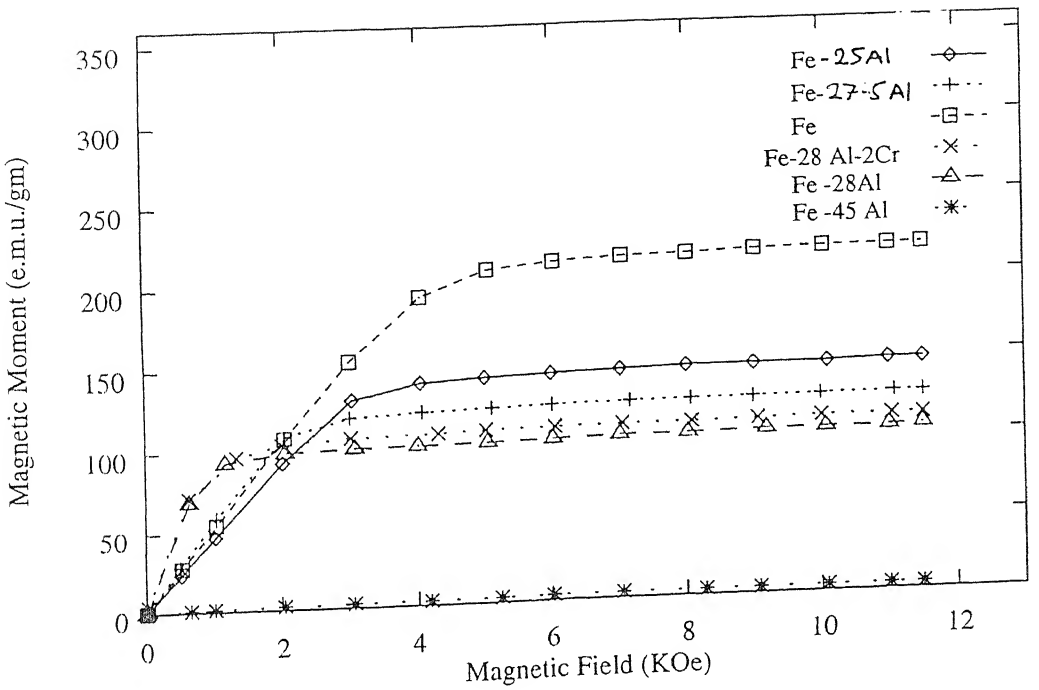

Figure 36. Effect of aluminium concentration and alloying on the magnetic saturation of iron aluminide.

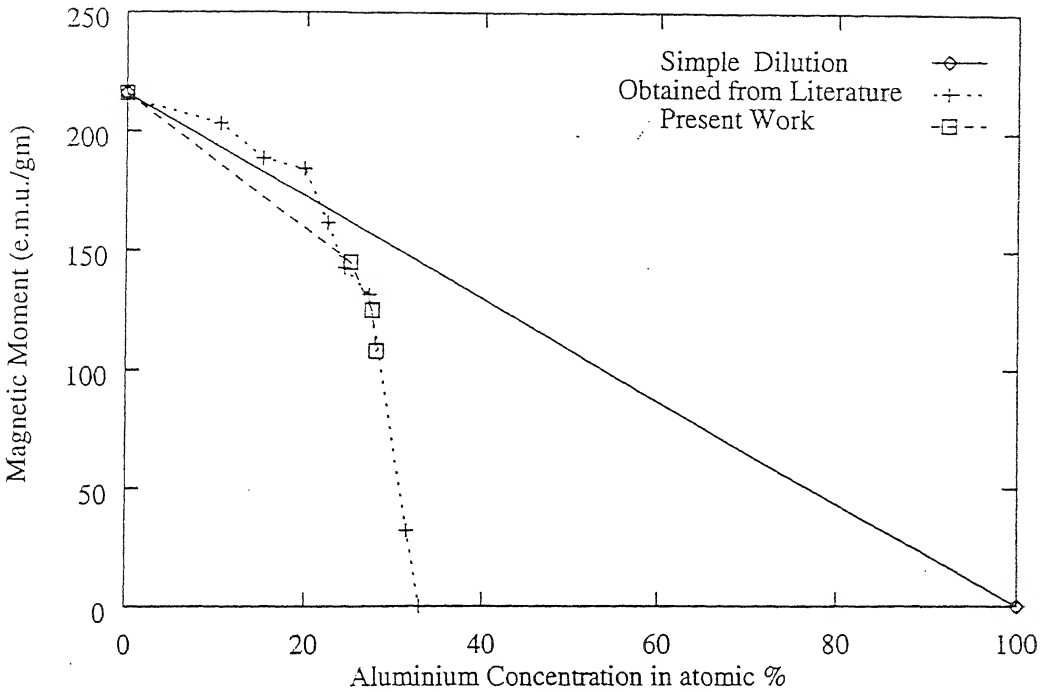

Figure 37. Effect of Aluminium concentration on magnetic saturation of iron aluminide compared with literature.

Table 8. Effects of hydrogen and alloying on saturation magnetization of iron aluminide.

Material	Treatment	Magnetic Saturation Ms at 300 K (e.m.u./gm)
Fe	Virgin	216
Fe-25Al Sample 1	Virgin	145
Fe-25Al Sample 2	Virgin	125
Fe-28Al	Virgin	108
Fe-28Al-2Cr	Virgin	114
Fe-45Al	Virgin	3.76
Fe-70Al	Virgin	00
Fe-25Al Sample 2	Cathodically H_2 charged 19.30 hrs.	125
Fe-25Al Sample 2	20 hrs.	125
Fe-25Al Sample 2	60 hrs.	133
Fe-28Al-2Cr	H_2 Gas charged 800^0C/3 hrs.	89
Fe-28Al	H_2 Gas charged 800^0C/3 hrs.	108
Fe-25Al Sample 1	H_2 Gas charged 800^0C/3 hrs.	145

Probably both these mechanisms are operative. On account of this about 0.8% reduction in both the iron and aluminium radii have been observed by these workers. The above postulate of d-shell absorption have been further substantiated by the neutron diffraction studies of magnetically ordered Fe_3Al. These workers [70] found that the tetrahydrelly surrounded iron atoms have approximately half the normal magnetic moment of iron namely 1.3+ - 0.15 Bhor magnetons while iron atoms at cube centers with the usual coordination of eight iron neighbors, possess a normal moment of 2.0 + - 0.15 μB.

It thus seem that when the critical amount of 22 atomic per cent aluminium is exceeded and the lattice become fully ordered, one third of the iron atoms have their moments reduced to nearly half the normal value.

At this stage further addition of Al atoms increases Fe-Fe separation leading to breakdown in Ferromagnetic interaction in addition to lowering of atomic magnetic moment to almost negligible value.

To resolve this point further we need neutron diffraction data over a whole series of iron-aluminium atoms and a data from soft x-ray absorption spectra which would give some insight into the nature of electron transfer.

4.6 EFFECT OF ELECTROLYTIC HYDROGEN CHARGING ON THE MAGNETIC SATURATION OF IRON ALUMINIDE

The results obtained are shown in the Figure 38 after different hydrogen charging treatment. No change in the saturation moment was observed for the 18 and 20 hours hydrogen charging. While there is only 7% increase in the magnetic saturation was observed after 60 hrs of cathodic hydrogen charging which either indicates that the hydrogen has diffused into the bulk of the material or the leaching of aluminium. While in the first two cases the hydrogen has not diffused into the bulk of

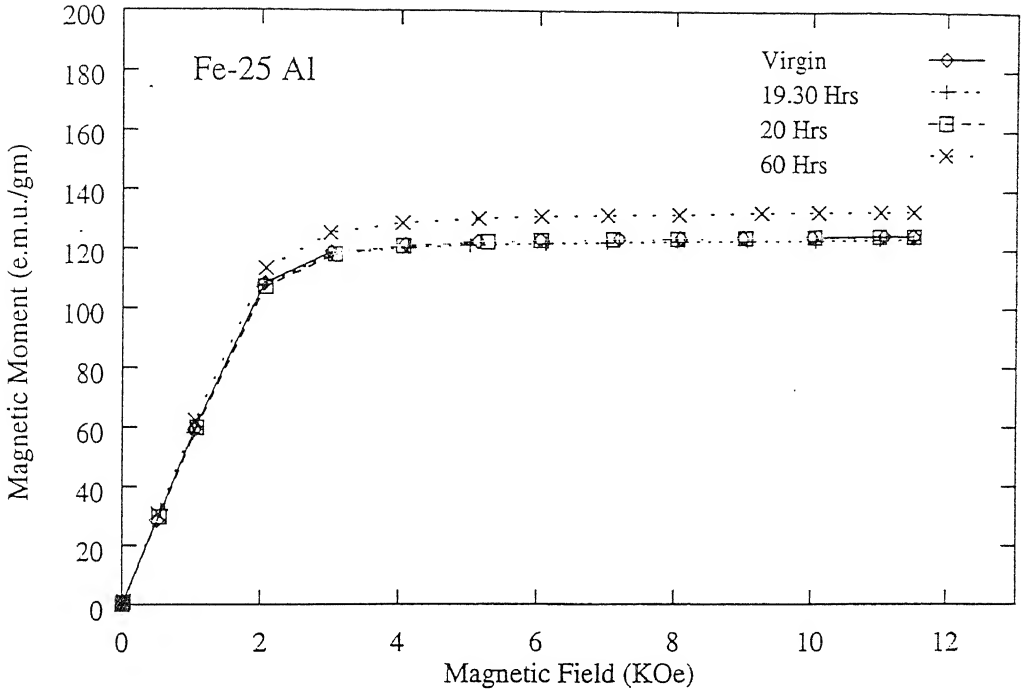

Figure 38. Effect of cathodic hydrogen charging on the magnetic saturation of iron aluminide charged in 0.1 N H_2SO_4 at a current density of 10mA/cm^2 for diffrent times.

the material and it is concentrated on the surface only and hence there is no noticeable change in the magnetic saturation was observed. This is substantiated by the ERDA spectra that the most of the hydrogen is concentrated near the surface.

4.7 EFFECT OF HIGH TEMPERATURE HYDROGEN CHARGING

Figure 39, Figure 40 and Figure 41 shows the effect of hydrogen charging at high temperature at 800^0C for 3 hrs. There is no change in the magnetic saturation of Fe-25Al and Fe-28Al is observed. This is in good agreement with the ERDA spectra obtained clearly indicated that the hydrogen concentration of 2.75% was found on the surface. Molecular hydrogen does not diffuse into the material easily. Hence the hydrogen has not diffused in the bulk of the material. The depth of diffusion being only 2000 ^{0}A or slightly more. Hence no noticeable change in the magnetic saturation is obtained.

The only exceptions to the above results is the Fe-28Al-2Cr sample. 22% decrease in the magnetic saturation was observed. This phenomenon should also occur with pure Fe_3Al. This aspect is yet not clear.

4.8 CURIE POINT DETECTION

Curie temperatures obtained in the present work is given in the table 9.

Material	Curie Temperature (^{0}C)
Fe-25 Al	581
Fe-28 Al	365
Fe-28 Al-2Cr	425

The curie temperature detected in our case is not the actual curie temperature but it is a phase boundary which separates the ordered Fe_3Al magnetic structure to the non magnetic FeAl ordered structure.

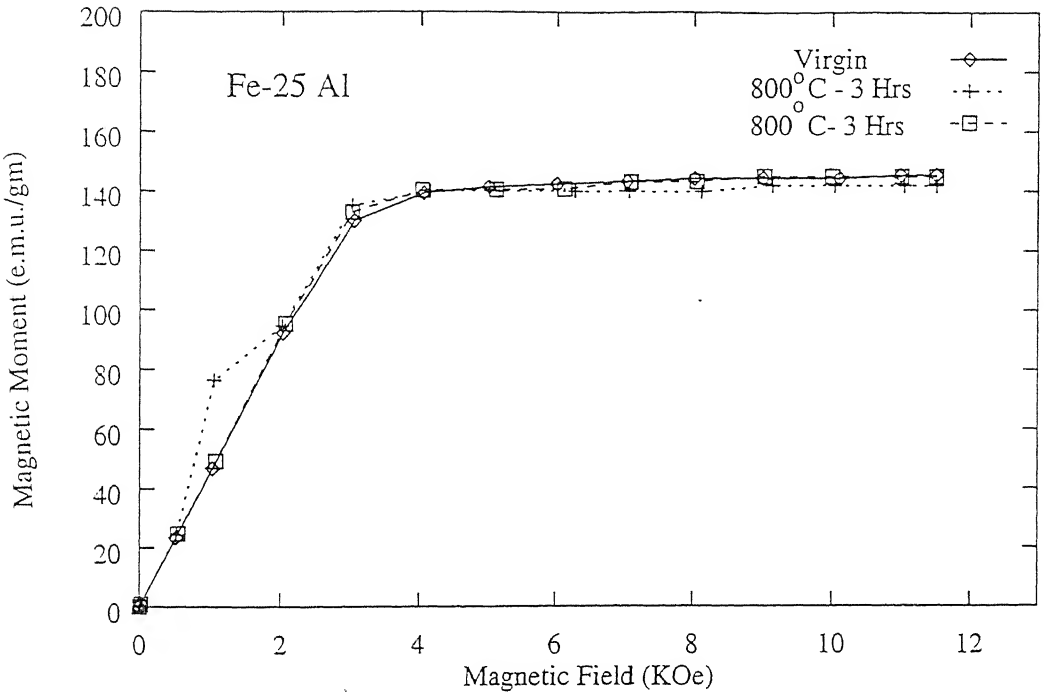

Figure 39. Effect of high temperature hydrogen charging on the saturation magnetization of Fe-25Al charged at 800^0 C for 3 hrs.

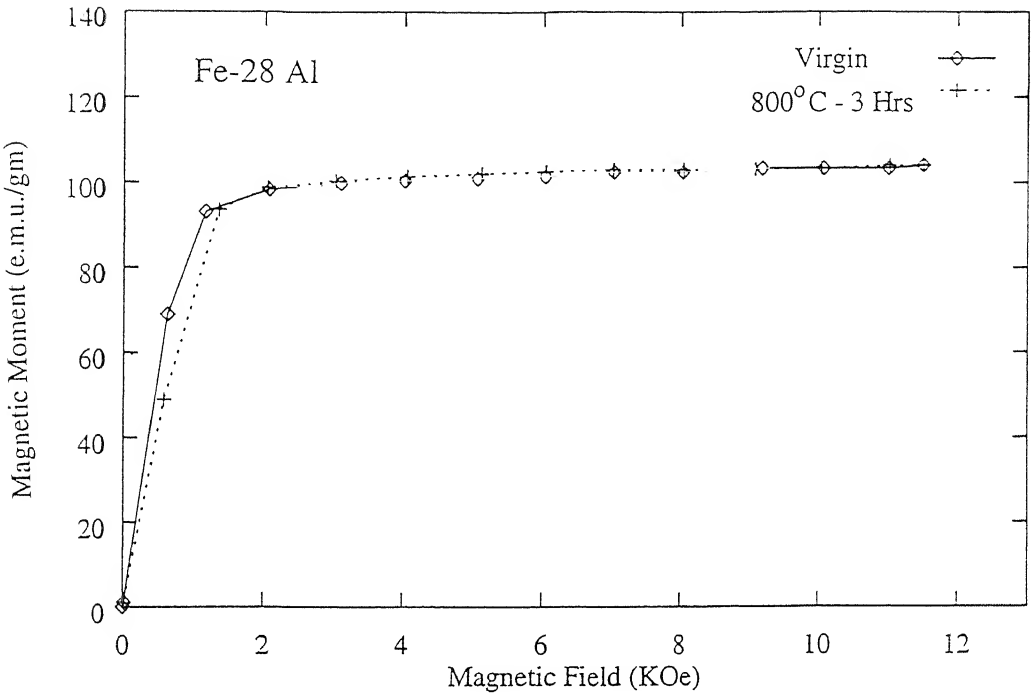

Figure 40. Effect of high temperature hydrogen charging on the saturation magnetization of Fe-28Al charged at 800^0 C for 3 hrs.

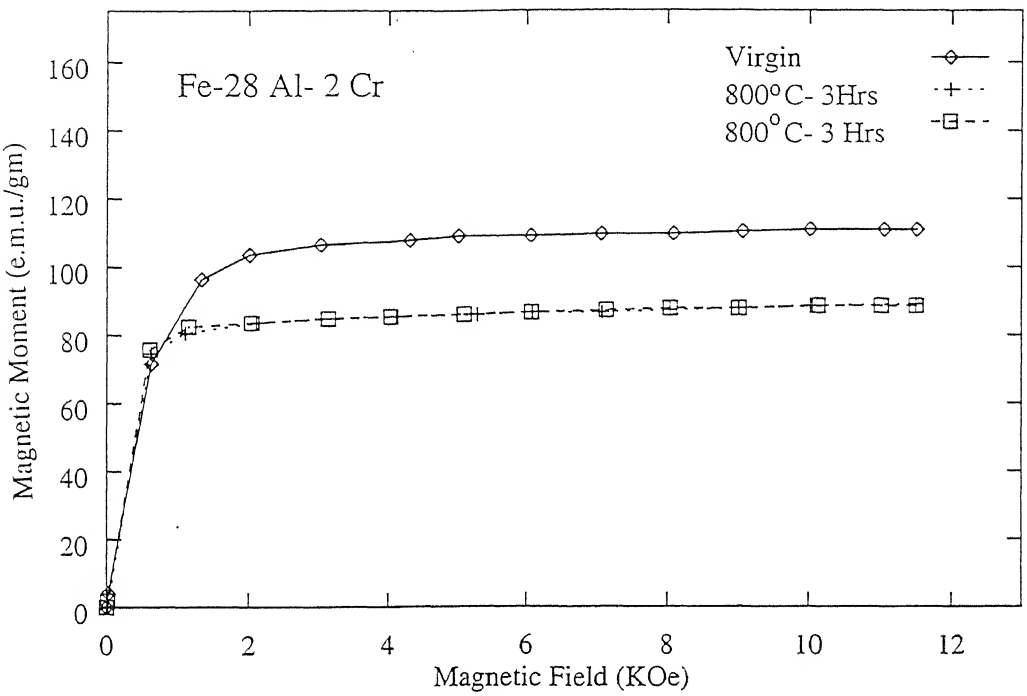

Figure 41. Effect of high temperature hydrogen charging on the saturation magnetization of Fe-28Al-2Cr charged at 800^0 C for 3 hrs.

Comparing the effect of chromium, it was found to increase the curie temperature which is nothing but the phase boundary separating these two structure.

Additions of Mo, Si, Ti, Cr to Fe-Al alloys with an aluminium contents in the range of 20 - 28Al% have been found to increase DO3 - B2 transition temperature by as much as 250^0 C over that binary Fe-Al alloys Tc 540^0C [73]. These increase in Tc have been related to increase in the ordering energies of DO3 superlattice caused by specific site substitution by the solutes. The study of verity of alloys both ternary and higher order has permitted development of an empirical expression relating transformation temperature to the amount of solutes and aluminium contents.

CHAPTER 5

SUMMARY

The salient conclusions of the present study with the suggested work for future are presented here.

5.1 CONCLUSIONS

I] We tried the depthwise study of hydrogen after cathodic hydrogen charging using elastic recoil detection analysis. The maximum depth for hydrogen diffusion was found to be 6 μm in 12 hrs in 0.1 N H_2SO_4 solution at 10 mA/cm^2 current density.

II] A rough estimate of hydrogen diffusion coefficient by using $x = \sqrt{Dt}$ gives the value to be lying between 8.33×10^{-16} - 1.15×10^{-17} m^2/s.

III] Plasma hydrogen charging and high temperature charging study implies that the molecular hydrogen is ineffective in diffusing into the aluminide only atomic and ionic hydrogen has tendency to diffuse easily into the material.

IV] Presence of hydrogen in the metallographically polished sample gives the evidence that the hydrogen is generated by the reaction of Fe 25Al with water. As water is used in polishing this high fugacity hydrogen generated must have diffused into the material while polishing the sample.

V] Thus there is probably direct evidence that the hydrogen is generated by the reaction of Fe-25Al with water and is one of the cause for the embrittlement of intermetallic.

HYDROGEN DESORPTION STUDY

I] Deuterium is completely removed at 450^0 C and there is no traces of deuterium after this treatment. This implies that the deuterium desorption temperature is lower than the hydrogen desorption.

II] It is not clear at present however whether the temperature ranges corresponding to the elimination of peaks coincide with the critical release temperature of hydrogen. Hydrogen releasing must be accompanied by the diffusion of hydrogen which is the time dependence process. Therefore the actual release temperature for hydrogen in vacancies and hydrogen in the lattice may be lower than the temperature ranges mentioned here.

III] These studies reflects that the embrittlement due to internal hydrogen in completely reversible. It also proves that heat treatment in vacuum is efficient to remove the hydrogen and only holding in conventional vacuum system at room temperature is not enough to eliminate internal hydrogen.

MAGNETIC MEASUREMENT

I] Near about 16% difference in the saturation values were obtained for two different Fe-25Al samples. This indicates that there is segregation in the material which led to the composition difference and ultimately affected the magnetic saturation.

II] Magnetic moment of iron aluminide falls in a linear fashion till 22 at per cent aluminium is reached and then the expected precipitous drop in the magnetic saturation value was observed.

III] High temperature hydrogen charging in Fe28Al2Cr at 800^0C/3hrs shows 22% decrease in the magnetic saturation . This aspect is not yet clear.

CURIE POINT DETECTION

I] The curie temperature detected in our case is not the actual curie temperature but it is a phase boundary which separates the ordered Fe_3Al magnetic structure to the non magnetic FeAl ordered structure.

II] None the less a strong conclusion can be drawn that the addition of chromium increases the DO3-B2 transition temperature and there by increases curie temperature.

5.2 SUGGESTIONS FOR FUTURE WORK

The following additional work needs to be undertaken in order to resolve some of the points.

I] Effect of various alloying additions like Cr, Ti, Si in iron aluminide on the hydrogen diffusion should be studied in greater detail using ERDA.

II] Desorption study of hydrogen needs to be carried out at least at three different temperatures to calculate the critical hydrogen release temperature.

III] The anomalous behaviour of iron aluminide after 22 atomic per cent aluminium should be resolved further with the neutron diffraction data over a whole series of iron-aluminium atoms and a data from soft x-ray absorption spectra which would give some insight into the nature of electron transfer.

IV] Effects of various alloying additions like Cr, Mo, W, Ti, Ni and Si on the DO3-B2 transformation temperature should be studied with the help of magnetic measurement.

REFERENCES

1. C. T. Liu and K. S. Kumar, "Ordered intermetallic alloys, Part 1: Nickel and Iron Aluminides", *J. Metals.* 45 (1993) 38-44.

2. C. Sykes and J Bampyfylde, "The physical properties of iron-aluminium alloys", *J. Iron Steel Inst.* 130 (1932) 389-394.

3. C. T. Liu, E. H. Lee and C. G. McKamey, "An environmental effect as the major cause for room temperature embrittlement in FeAl", *Scripta Metall.* 23 (1989) 875-880.

4. Y. F. Zhu, D. T. Liu, C. H. Chen, "Direct evidence of hydrogen generation from the reaction of water with FeAl", *Scripta Mater.*, 35 (1996) 1435-1439.

5. C. T. Liu, C. G. McKamey and E. H. Lee, "Environmental effects on room temperature ductility and fracture mode in Fe_3Al", *Scripta Metall. Mater.* 24 (1990) 385-390.

6. C. G. McKamey, J. A. Horton and C. T. Liu, "Effect of Chromium on room temperature ductility and fracture mode in Fe_3Al", *Scripta Metall.* 22 (1988) 1679-1681.

7. C. G. McKamey and C. T. Liu, "Chromium addition and environmental embrittlement in Fe_3Al", *Scripta Metall. Mater.* 24 (1990) 2119-2122.

8. R. Balasubramaniam, "On the role of chromium in minimizing room temperature hydrogen embrittlement in iron aluminides", *Scripta Mater.* 34 (1996) 127-133.

9. Zhang Zhonghua, Sun Yangshan, Liu Guijun and Guo Jun, "Ductility Improvement of Fe_3Al based alloy with surface coating', ***Scripta Mater.***, 35 (1996) 1071-1075.

10. A. Agarwal, R. Balasubramaniam and S. Bhargava, "Effect of Thermomechanical treatments on the room temperature mechanical behavior of iron aluminide Fe_3Al", ***Met. Mater. Trans A***, 27A (1996) 2985-2994.

11. R. Balasubramaniam, "Alloy Development to minimize room temperature hydrogen embrittlement in iron aluminides", ***J. Alloys and Comp.***, (1997) in press.

12. A. Agarwal and R. Balasubramaniam, "Role of surface passive films on the hydrogen embrittlement of iron aluminides", ***Bull. Mater. Sci.***, 19 (1996) 91-102.

13. A. Agarwal, M. J. Akhtar and R. Balasubramaniam, "Effect of alloying on aqueous corrosion and mechanical behavior of iron aluminide Fe_3Al", ***J. Mat. Sci.*** 31 (1996) 5207-5213.

14. A. Agarwal and R. Balasubramaniam, "Hall-Petch behavior of stoichiometric Fe_3Al", ***J. Mat. Sci. Lett.*** (1997) in press.

15. C. G. McKamey and D. H. Pierce, "Effect of recrystallization on room temperature tensile properties of an Fe_3Al based alloy", ***Scripta Metall. mater*** 28, (1993) 1173-1176.

16. C. Thakur and R. Balasubramaniam, "Determination of hydrogen diffusivity in Al-Li-Cu-Mg alloys", ***J. Mater. Sci. Lett.*** 15 (1996) 1397-1399.

17. P. Kumar and R. Balasubramaniam, "Determination of hydrogen diffusivity in austenitic stainless steels by subscale microhardness profiling", ***J. Alloys Compounds***, (1997) in press.

18. P. Banergee Thesis, "Hydrogen behaviour in chromium and titanium alloyed iron aluminide", (1997) I.I.T. Kanpur.

19. M. A. Crimp and K. M. Vedula, "Effect of boron on the tensile properties of B2 FeAl", *Mat. Sci. Eng.* 78, (1986) 193-199.

20. C. T. Liu and E. P. George, "Environmental embrittlement in boron free and boron doped FeAl alloys", *Scripta Metall. Mater.* 24, (1990) 1285-1290.

21. D. Lin, A. Shan and D. Li, "Super plasticity in Fe_3Al based alloy with large grains", *Scripta. Metall. Mater.* 31 (1994) 1445-1460.

22. S. Yangshan, Y. Zhengiun, Z. Zhonghua and H. Haibo, "Mechanical properties of Fe_3Al based alloys with cerium addition", *Scripta Metall. Mater.* 33 (1995) 811.

23. P. Banergee and R. Balasubramaniam, "Effect of Mischmetal addition on the mechanical behaviour of chromium and titanium alloyed iron aluminides", *Scripta. Metall. Mater.* (1997) communicated.

24. J. H. Schneibel, "Selected properties of iron aluminides", ***Processing, properties and Applications of Iron Aluminides***; eds. J. H. Schneibel and M. A. Crimp, TMS, Warrendale, USA, (1994) 335.

25. R. J. Lynch, K. A. Gee and L. A. Held, "Environmental embrittlement of single crystals and thermomechanically processed B2 ordered iron aluminides", *Scripta. Metall. Mater.* 30 (1994) 945-950.

26. D. G. Morris and M. Leboeuf, "The role of controlled recrystallisation treatment on ductility of Fe_3Al alloys", *Acta. Metall. Mater.* 42 (1994) 1817-1823.

27. Y. H. Lu, Z. Q. Hung and H. Zhang, "Effect of heat treatment on temperature on the tensile properties of a Fe-28Al-5Cr-0.313B-0.003Mg alloy", *Scripta. Metall. Mater.* 33 (1995) 609-613.

28. Y. Yangand I. Baker "Recrystallisation of FeAl and Ni_3Al with and without boron", *Scripta. Metall. Mater.* 34 (1996) 803-807.

29. S. Visvanathan, B. R. Shelton, J. K. Wright and V. K. Sikka "Effect of thermomechanical processing on the room temperature tensile properties of Fe_3Al based alloys", *Scripta. Metall. Mater.* 29 (1993) 589-594.

30. I. Baker and D. J. Gyadesh, "Dynamic recrystallisation and grain boundary migration in B2FeAl", *Mettalography.* 20 (1987) 347-357.

31. C. G. McKamey, J. H. devan, P. F. Tortorelli and V. K. Sikka, "A review of recent development in Fe_3Al based alloy", *J. Mater. Res.* 6 (1991) 1779-1786.

32. G. Zhu, W. Mao, Y. Yu and Z. Sun, "Driving forces and recrystallisation behaviour of Fe-28Al-5Cr alloy", ***International Seminar on Texture*** (1996) 1088-1092.

33. Bevis Hutchinson, Steffen Jhonson and lena Ryde, "On the kinetics of recrystallisation in the cold worked metals", *Scripta. Metall. Mater.* 23 (1989) 671-676.

34. Junpin Lin, Wuang Chu and Chimei hasio, "Hydrogen induced cracking in Fe_3Al-Cr", *Scripta. Metall. Mater.* 30 (1994) 583-586.

35. J. C. M. Li and T. Liu, "Crack nucleation in hydrogen embrittlement", *Scripta. Metall. Mater.* 27 (1992) 1701-1705.

36. A. Agarwal and R. Balasubramaniam, "Fracture characteristics of alloyed iron aluminides", *Pract. Metallogr.* 33 (1996) 453-466.

37. R. W. Cahn, "Physical Metallurgy", American Elsevier Publishing Company, Inc., NEWYORK, (1965) 471-584.

38. J. Volkl and G. Alefeld, "Diffusion of hydrogen in metals", ***Topics in Applied Physics***, 28 (1978) 321-344.

39. J. Volki and G. Alefeld, in ***Diffusion in Solids***, edited by A. S. Nowick and J. J. Burton, Academic Press, New York, USA, (1975) 231.

40. M. Hasaka, T. Murimura, S. Kondo, Y. Yuchiyama and K. Hisastune, "Diffusion of boron in order Fe-26 at%Al", ***Scripta. Metall. Mater.*** 29 (1993) 967-970.

41. M. Hasaka, R. Murimora, S. Kondo, Y. Yuchiyama, H. Nakashima and K. Hisastune, "Diffusion of nickel, vanadinum and titanium in order Fe-26 at%Al", ***Scripta. Metall. Mater.*** 29 (1993) 963-966.

42. J. Bernandini, Z. S. Tokeu, P. Gas and D. L. Beke, "Volume diffusion of iron in Fe_3Al:influence of ordering", ***Scripta. Metall. Mater.*** 45 (1997) 541-546.

43. K. Kiuchi and R. B. McLellan, "The solubility and diffusivity of hydrogen in well- annealed and deformed iron", ***Acta Metall.*** 31 (1983) 961-984.

44. M. Nagano, Y. Hauyshi, N. Ohtni, M. Issihiki and K. Igaki, "Hydrogen diffusity in high purity α-iron", in ***Perspectives in Hydrogen in Metals***, edited by M. F. Ashby and J. P. Hirth, (1986) 255-259.

45. A. Troino Festchrift, "Hydrogen embrittlement and stress corrosion cracking", edited by R. Giballa and R. F. Henemann (1984).

46. A troino, ***Trans. ASM*** 52 (1960) 54.

47. J. P. Hirth, "Effect of hydrogen on the properties of iron and steel", ***Met. Trans.*** 11A (1980) 861-890.

48. H. H. Jhonson, "Hydrogen in iron", *Met. Trans.* 19A (1988) 2371.

49. T. Tabata and H. K. Birnbaum, "Direct observation of the hydrogen enhanced crack propogation in iron", ***Perspective in Hydrogen in Metals***, 723-729.

50. G. M. Pressouyre, "A classification of hydrogen traps in steel", communication, *Met. Trans.* 10A (1979) 1571-1573.

51. D. A. Jones, "Principle and prevention of corrosion", Maxwell McMillan International Publishing Group, NEWYORK, USA (1992).

52. A. I. Shirley and C. K. Hall, "Trapping of hydrogen by substitutional and interstial impurites in α-iron", ***Perspectives in Hydrogen in Metals***, 381-386.

53. G. M. Pressouyre and I. M. Bernstem, "An electrical anology model of hydrogen trapping in iron alloys", *Corrosion Science.* 18 (1978) 811-833.

54. N. R. Gleason, C. A. Gerken and D. R. Strongin, *Applied Surface Science* 72 (1993) 215.

55. W. Y. Choo and Jai Young Lee, "Thermal analysis of trapped hydrogen in pure iron", *Met. Trans.* 13A (1982) 135-140.

56. Y. Yang and S. Hanada, "Absorption and desorption of hydrogen in Fe-40Al intermetallic", *Scripta. Metall. Mater.* 32 (1995) 1719-1724.

57. X. Y. Huang, W. Mader and R. Kirchheim, "Hydrogen and oxygen at metal/oxide interlatics", *Acta. Met.* 39 (1991) 893-907.

58. Govind, R. Balasubramaniam and G. S. Upadhyay, "Effect of hydrogen on the ductility of ODS copper", *Scripta. Metall. Mater.* 29 (1993) 1303-1308.

59. Reiner Kircheim, "Hydrogen solubility and diffusivity in defective and amorphous metal", *Progress in Material Science*, 32 (1988) 261-325.

60. Gye-Won Hong and Jai Young Lee, "The interaction of hydrogen with dislocation in iron", ***Perspectives in Hydrogen in Metals***, 427-435.

61. A. J. Kumnik and H. H. Jhonson, "Deep trapping states for hydrogen in deformed iron", *Acta. Met.* 28 (1980) 33-39.

62. T. Tabata and H. K. Birnbaum, "Direct observation of the effect of hydrogen on the behaviour of dislocations in iron", ***Perspectives in Hydrogen in Metals***, 581-585.

63. T. Mastumoto, J. Eastaman and H. K. Birnbaum, "Direct observation of enhanced dislocation mobility due to hydrogen", ***Perspectives in Hydrogen in Metals***, 723-729.

64. H. Chiu, L. Qiao and X. Mao, "Environment assisted cracking of iron aluminide in 3.5% NaCl solution", ***Scripta. Metall. Mater.*** 25 (1996)963-969.

65. D. Kasual and L. Heldt, "Effect of environment on themechanical properties of an Fe-24.6Al alloy", ***Scripta. Metall. Mater.*** 25 (1991) 1047-1051.

66. H. K. Birnbaum, G. M. Bond and I. M. Robertson, "Effect of hydrogen on determation and fracture processes in high purity aluminium", ***Acta. Metall.*** 36 (1988) 2193-2198.

67. N. S. Stoloff and D. J. Duquettee, "Moisture and hydrogen induced embrittlement of iron aluminides", ***J. Metall.*** 45 (1993) 30-35.

68. I. Baker and P. Munroe, "Observation of <100> dislocations and a mechanism for transgannular fracture", ***Acta. Metall. mater.*** 39 (1991) 1011-1017.

69. A. Taylor and R. M. Jones, "Constitution and magnetic properties of iron-rich iron-aluminium alloys", ***J. Phys. Chem. Solids*** 16 (1958) 16-32.

70. Sykes C. and Evans H. ***J. Iron Steel Institute*** 125 (1935) 225.

71. X. Mao and L. Qiao, "On the nanocrack nucleation and propogation mechanisms of Fe_3Al intermetallics", ***Acta. Mater.*** 44 (1996) 2327-2335.

72. W. M. Muller, J. P. Blackledge and G. G. Libowitz, "Metal Hydrides", Academic press, New York, London (1968).

73. R. T. Fortnum and D. E. Mikkola, "Effects of Molybdenum, Titanium and Silicon additions on the $DO_3 \rightarrow B2$ transition temperature for alloys near Fe_3Al", ***Materials Science and Engineering***, 91 (1987) 223-231.

.....	....
.....	....
.....	....
.....	....
.....	....
.....	....
.....	....
.....	....
.....	....
.....	....
.....	....